Unclassified

SECURITY CLASSIFICATION OF THIS PAGE

REPORT DOCUMENTATION PAGE

Form Approved OMB No. 0704-0188

1a. REPORT SECURITY CLASSIFICATION: Unclassified	1b. RESTRICTIVE MARKINGS
2a. SECURITY CLASSIFICATION AUTHORITY	3. DISTRIBUTION/AVAILABILITY OF REPORT: Approved for public release; Distribution unlimited
2b. DECLASSIFICATION/DOWNGRADING SCHEDULE	
4. PERFORMING ORGANIZATION REPORT NUMBER(S): GL-TR-90-0185	5. MONITORING ORGANIZATION REPORT NUMBER(S)
6a. NAME OF PERFORMING ORGANIZATION: Geophysics Laboratory; 6b. OFFICE SYMBOL (If applicable): PHG	7a. NAME OF MONITORING ORGANIZATION
6c. ADDRESS (City, State, and ZIP Code): Hanscom AFB, Massachusetts 01731-5000	7b. ADDRESS (City, State, and ZIP Code)
8a. NAME OF FUNDING/SPONSORING ORGANIZATION; 8b. OFFICE SYMBOL (If applicable)	9. PROCUREMENT INSTRUMENT IDENTIFICATION NUMBER
8c. ADDRESS (City, State, and ZIP Code)	10. SOURCE OF FUNDING NUMBERS

PROGRAM ELEMENT NO	PROJECT NO	TASK NO	WORK UNIT ACCESSION NO
61102F	2311	G5	02

11. TITLE (Include Security Classification)
Northward IMF and Patterns of High-Latitude Precipitation and Field-Aligned Currents: The February 1986 Storm

12. PERSONAL AUTHOR(S)
F.J. Rich, D.A. Hardy, R.H. Redus, M.S. Gussenhoven

13a. TYPE OF REPORT	13b. TIME COVERED	14. DATE OF REPORT (Year, Month, Day)	15. PAGE COUNT
Reprint	FROM _____ TO _____	1990 July 30	24

16. SUPPLEMENTARY NOTATION
Reprinted from Journal of Geophysical Research, Vol. 95, No. A6, pages 7893-7913, June 1, 1990

17. COSATI CODES		
FIELD	GROUP	SUB-GROUP

18. SUBJECT TERMS (Continue on reverse if necessary and identify by block number)
Field aligned currents, Aurora, Polar cap arcs, DMSP(Defense Meteorology Satellite Program) Geomagnetic Storm

19. ABSTRACT (Continue on reverse if necessary and identify by block number)

On February 7, 1986, during a major geomagnetic storm the B_z component of the interplanetary magnetic field (IMF) turned strongly northward for several hours. Data from the Defense Meteorological Satellite Program F6 and F7 satellites and the HILAT satellite were used to study the evolution of the pattern of high-latitude precipitation and field-aligned currents in response to this change. Prior to the northward IMF period, the auroral zone was observed down to mid-latitudes and was very wide in latitude, and strong, large-scale region 1 / region 2 currents were clearly present ($\Delta B \sim 1700$ nanoteslas). Following the northward turning, the equatorward boundary of the auroral zone on the nightside contracted sharply poleward and polar cap arcs were observed. The strength of the region 1 / region 2 currents decreased markedly and became immeasurably small at the time of the maximum contraction of the auroral oval. An NBZ current system was observed to grow and expand in the southern (summer) high latitude region over a period of more than 2 hours. Simultaneously, an irregular pattern of field-aligned currents was observed in the northern (winter) hemisphere. During the contraction, the latitudinal width of the auroral region mapping to the central plasma sheet (CPS) decreased dramatically while the

(Cont'd)

20. DISTRIBUTION/AVAILABILITY OF ABSTRACT	21. ABSTRACT SECURITY CLASSIFICATION
☐ UNCLASSIFIED/UNLIMITED ☒ SAME AS RPT. ☐ DTIC USERS	Unclassified

22a. NAME OF RESPONSIBLE INDIVIDUAL	22b. TELEPHONE (Include Area Code)	22c. OFFICE SYMBOL
F.J. Rich	(617) 377-2431	PHG

DD Form 1473, JUN 86 — Previous editions are obsolete. — SECURITY CLASSIFICATION OF THIS PAGE: Unclassified

Cont of Block 19:

width of the area mapping to the boundary plasma regions (BPR) in the magnetosphere increased greatly. At the time of the maximum contraction the BPR extended up to a latitude of at least 87.1°. The NBZ currents expanded wi and were entirely located within the BPR precipitation. Polar cap arcs were observed in both regions of BPR precipitation and polar cap precipitation and were not correlated with the location of the large-scale field-aligned currents. There was no indication of the CPS intruding to high latitudes, and thus no evidence for bifurcation of the magnetotail. The boundary between the CPS and the BPR showed little change. If this implies that the boundary between open and closed field lines contracted slowly or not at all, then a significant portion of the observed BPR precipitation was observed along open field lines. We interpret the pattern of particle precipitation and field-aligned current and the implied plasma convection in terms of a distorted, two-cell convection pattern driven by merging of closed field lines with the IMF as proposed by Crooker [1988]. When the IMF turned southward again, the pattern quickly reversed. The BPR contracted; the CPS precipitation regions expanded; the equatorward boundary of the auroral oval moved to lower latitudes; the NBZ currents disappeared in less than 30 min; and the region 1 / region 2 currents reappeared. Again, the BPR/CPS boundary did not move as rapidly and thus may indicate that the changes are due more to a reconfiguration within the magnetosphere than a change in the portion of the magnetosphere that is open or closed.

JOURNAL OF GEOPHYSICAL RESEARCH, VOL. 95, NO. A6, PAGES 7893-7913, JUNE 1, 1990

Northward IMF and Patterns of High-Latitude Precipitation and Field-Aligned Currents: The February 1986 Storm

F. J. RICH, D. A. HARDY, R. H. REDUS, AND M. S. GUSSENHOVEN

Geophysics Laboratory, Hanscom Air Force Base, Bedford, Massachusetts

On February 7, 1986, during a major geomagnetic storm the B_z component of the interplanetary magnetic field (IMF) turned strongly northward for several hours. Data from the Defense Meteorological Satellite Program F6 and F7 satellites and the HILAT satellite were used to study the evolution of the pattern of high-latitude precipitation and field-aligned currents in response to this change. Prior to the northward IMF period, the auroral zone was observed down to mid-latitudes and was very wide in latitude, and strong, large-scale "region 1 / region 2" currents were clearly present (ΔB ~1700 nanoteslas). Following the northward turning, the equatorward boundary of the auroral zone on the nightside contracted sharply poleward and polar cap arcs were observed. The strength of the region 1 / region 2 currents decreased markedly and became immeasurably small at the time of the maximum contraction of the auroral oval. An NBZ current system was observed to grow and expand in the southern (summer) high latitude region over a period of more than 2 hours. Simultaneously, an irregular pattern of field-aligned currents was observed in the northern (winter) hemisphere. During the contraction, the latitudinal width of the auroral region mapping to the central plasma sheet (CPS) decreased dramatically while the width of the area mapping to the boundary plasma regions (BPR) in the magnetosphere increased greatly. At the time of the maximum contraction the BPR extended up to a latitude of at least 87.1°. The NBZ currents expanded with and were entirely located within the BPR precipitation. Polar cap arcs were observed in both regions of BPR precipitation and polar cap precipitation and were not correlated with the location of the large-scale field-aligned currents. There was no indication of the CPS intruding to high latitudes, and thus no evidence for bifurcation of the magnetotail. The boundary between the CPS and the BPR showed little change. If this implies that the boundary between open and closed field lines contracted slowly or not at all, then a significant portion of the observed BPR precipitation was observed along open field lines. We interpret the pattern of particle precipitation and field-aligned current and the implied plasma convection in terms of a distorted, two-cell convection pattern driven by merging of closed field lines with the IMF as proposed by Crooker [1988]. When the IMF turned southward again, the pattern quickly reversed. The BPR contracted; the CPS precipitation regions expanded; the equatorward boundary of the auroral oval moved to lower latitudes; the NBZ currents disappeared in less than 30 min; and the region 1 / region 2 currents reappeared. Again, the BPR/CPS boundary did not move as rapidly and thus may indicate that the changes are due more to a reconfiguration within the magnetosphere than a change in the portion of the magnetosphere that is open or closed.

1. INTRODUCTION

Depending on the sign of the z component of the interplanetary magnetic field (IMF) in solar-magnetospheric coordinates, different dynamical states are established within the auroral zone and polar cap and in their associated regions in the magnetosphere. When the IMF B_z component is negative (southward), moderate to intense levels of particle precipitation occur within the auroral zone associated with an increased level of substorm activity. Simultaneously at latitudes above the auroral zone the smooth and slowly varying precipitation of polar rain is observed across the polar cap [*Heikkila*, 1972; *Winningham and Heikkila*, 1974; *Winningham et al.*, 1975; *Gussenhoven et al.*, 1984]. Well-defined "region 1 / region 2" field-aligned currents flow into and out of the auroral zone, but no large-scale field-aligned currents occur in the polar cap [*Iijima and Potemra*, 1976]. The electric field can exhibit large spatial gradients in magnitude across the polar cap but generally is oriented dawn to dusk such that there is convection antisunward in this region with sunward convection within most of the auroral zone [*Reiff and Burch*, 1985 and references therein; *Heppner and Maynard*, 1987].

When the IMF B_z component is positive (northward), the intensity of precipitation within the auroral zone is generally lower, and the level of substorm activity is decreased. At the same time, there is enhanced precipitation in the polar cap in the form of "polar showers" or "polar squalls" [*Winningham and Heikkila*, 1974; *Hardy*, 1984] associated with both visual and subvisual Sun-aligned arcs [*Whalen et al.*, 1971; *Meng*, 1976; *Ismail et al.*, 1977; *Meng*, 1981; *Burke et al.*, 1982; *Gussenhoven*, 1982; *Hardy et al.*, 1982; *Frank et al.*, 1982; *Peterson and Shelley*, 1984; *Frank et al.*, 1986]. In the unilluminated polar cap the electric field is highly variable and structured with many small-scale reversals in orientation while in the sunlit polar cap the electric field is more smoothly varying with an extended region of sunward convection [*Burke et al.*, 1979]. Large-scale currents in the polar cap, known as the NBZ system, are observed toward the dayside of the cap, and more small-scale currents toward the nightside of the cap [*Iijima et al.*, 1984; *Iijima and Shibaji*, 1987].

Recently, an additional state has been suggested [*Rich and Gussenhoven*, 1987; *Hoffman et al.*, 1988; *Gussenhoven*, 1988] occurring when the IMF B_z component is small to slightly positive (−1 nT to +2 nT) and the total magnetic field magnitude and solar wind speed are low. For this state the auroral zone region 1 / region 2 currents are much diminished in intensity or immeasurably small. The field-aligned currents associated with the cusp continue almost

Paper number 89JA02964.

unchanged and the level of particle precipitation, especially that due to field-aligned accelerations in both the auroral zones and polar cap, is low.

For northward IMF, previous investigations have tended to concentrate on one aspect of these processes, e.g. the magnetic field, electric field or particle variations, or on the characteristics once the B_z northward state is achieved. In this paper, by contrast, we look at the simultaneous changes in the pattern of particle precipitation and field-aligned currents for a short period during the large geomagnetic storm of February 6-9 1986, when there was a marked transition between these states produced by a northward turning of the IMF. By combining data from two Defense Meteorological Satellite Program (DMSP) satellites and the HILAT satellite a picture is obtained of the global reconfiguration of the plasma regions in the auroral zone and polar cap and the relationship of that reconfiguration to the changes in the large scale system of field-aligned currents. We are able to follow the transition with the IMF changes because the transition occurred over a period long compared to the DMSP and HILAT orbital periods.

The magnitudes of the solar wind and IMF parameters were very large during the period we report on. As a result, the convection, field-aligned currents and particle precipitation driven by the interaction of the solar wind-magnetosphere-ionosphere were unusually large. We assume, nonetheless, that the nature of the interaction is not different than in normal times and that the increased magnitude contributes only to easier recognition of many defining features. In particular, we follow the boundary plasma dynamics to show how the boundary plasma region expands to very high latitude together with the appearance of the NBZ currents.

Following the introduction, we describe the instrumentation used and the satellite orbits in section 2. Section 3 contains an overview of the geomagnetic storm of February 6-9, 1986, the change in the field-aligned currents during the oval contraction and subsequent expansion, and the behavior of the precipitating electrons and ions during this period. Section 4 is the discussion, and section 5 the conclusions.

2. Instrumentation and Satellite Orbit

Data from instruments on the Defense Meteorological Satellite Program F6 and F7 satellites and the U. S. Air Force/Defense Nuclear Agency HILAT satellite were used in this study. The DMSP data are available continuously in the interval of interest. The HILAT satellite has no on-board recorder, so that data are available only in the northern hemisphere within sight of the ground recording stations. The tracks of the satellites in geomagnetic latitude and magnetic local time during the time of interest are shown in Figure 1. The DMSP F6 and F7 satellites were both in circular, 840-km altitude, polar, sun-synchronous orbits in the dawn-dusk and in the 1030 - 2230 hours local time meridians, respectively. The HILAT satellite was in a nearly circular (790–860 km altitude) polar orbit at an inclination of 83.2°. The HILAT orbital plane precesses in local time such that on February 8, 1986, the orbit was approximately coplanar with that for the DMSP F6 satellite in the dawn-dusk meridian. During the period of interest the two DMSP satellites' orbits were out of phase by approximately one half of the orbital period such that they passed over opposite high-latitude regions within 10 min of each other. The F7 and HILAT orbits were approximately in phase such that they passed over the northern high-latitude region within a few minutes of each other. For the period studied in this paper we examined in detail three full orbits of data from each of the DMSP satellites and two north pole passes from the HILAT satellite.

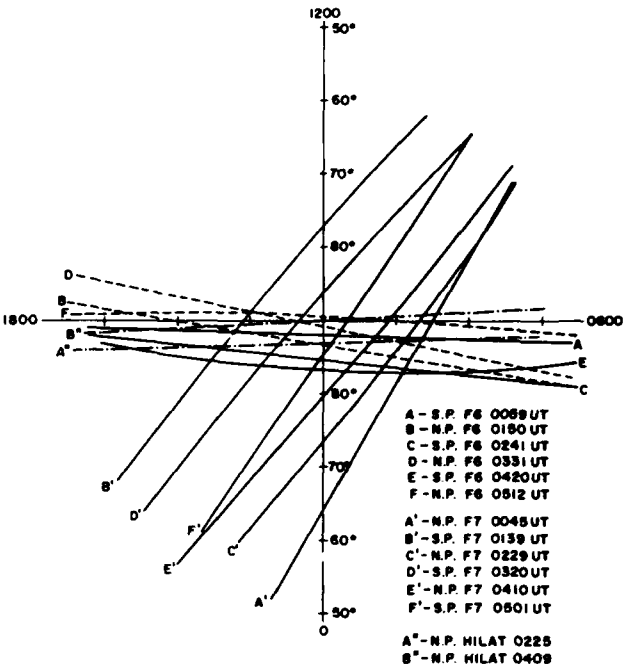

Fig. 1. Track of the DMSP F6, DMSP F7 and HILAT satellites in geomagnetic coordinates through the northern and southern high latitude regions during the period of study on February 8, 1986.

The SSJ/4 detectors on the DMSP satellites provided the particle data. Each of these curved-plate particle spectrometers returns a 20-point spectrum for both electrons and ions over the energy range from 30 eV to 30 keV once per second. The detectors measure the flux in a single direction and are oriented on the three-axis-stabilized satellite with their look directions toward the local zenith. (For more information see *Hardy et al.*, [1984a].)

For the HILAT satellite the particle data are from the J sensor. This instrument consists of an array of six analyzers configured to provide a 16-point electron spectrum over the energy range from 20 eV to 20 keV in three directions. This satellite is also three-axis stabilized, and the instrument is mounted with look directions approximately toward the local zenith, 40° from the local zenith and toward the local nadir. During the period studied in this paper, the J sensor was operating in a mode where only the spectrum from the zenith was being measured 12 times per second. (For more information see *Hardy et al.*, [1984b].).

Magnetic field data are available from magnetometers on the DMSP and HILAT satellites. Both satellites carried triaxial flux-gate magnetometers that return 20 vector measurements of the field each second. For this study only the DMSP magnetic field data were used. For more information, see *Rich* [1984]. The DMSP magnetometer data are given in spacecraft coordinates where x is downward in a local vertical system, y is parallel to the spacecraft velocity vector (approximately in the north/south direction) and z is perpendicular to the orbit plane in the sunward direction (approximately in the east/west direction). The magnetometer data are used then to infer field-aligned currents,

$$J_{\parallel} = J_x = \nabla_x \times \Delta B/\mu_o$$

If the infinite current sheet approximation is used, then

$$J_{\parallel} \simeq \frac{1}{\mu_o}\frac{\partial \Delta B_z}{\partial y}$$

If we assume that the field-aligned currents are largely due

to gradients in the ionospheric Pedersen currents, or

$$J_{\parallel} = \nabla \cdot J_P$$

then the electric field and the magnetic deflection vectors are related by

$$\Delta B_z/\mu_o = \Sigma_P\, E_y$$

$$\Delta B_y/\mu_o = \Sigma_P\, E_z$$

If the ionospheric conductivity is uniform, then a map of ΔB vectors is proportional to a map of plasma drift vectors.

The images of the aurora from the DMSP satellites are provided by the white light portion of the operational line scanner (OLS) with the aid of a photomultiplier tube. The images are built by scanning 7 times per second perpendicular to the velocity vector. At nadir, the pixel resolution is approximately 1 km by 1 km. Details of the white light imaging system were described by *Eather* [1979].

3. Observations

3.1. *Overview of Observations and Field-Aligned Current Variations*

A large geomagnetic storm occurred between February 6, 1986 and February 10, 1986 [*Allen*, 1986]. The K_p and D_{st} indices, which chart the course of the storm within the magnetosphere, along with the solar wind conditions are shown in Figure 2. The interplanetary data are incomplete due to low duty cycle of the IMP 8 satellite. Despite the interplanetary data being incomplete, these data show that this storm was driven by a significant and sustained increase in the energy impacting the magnetosphere from the interplanetary medium.

Starting midday on February 6, K_p began to increase reaching a peak value of 9 late on February 8. The K_p increase was accompanied by a general advance of the auroral equatorward boundary to lower latitudes. Using the DMSP data from two satellites and with four auroral crossings per orbit, we can continually follow this advance with a resolution of 25 min or less. This is best done by calculating the midnight boundary index or the equatorward edge of the electron precipitation along the midnight meridian estimated by the method given by *Gussenhoven et al.* [1983] and *Hardy et al.* [1985]. In calculating the midnight boundary index the individual boundaries are extrapolated to midnight eliminating the local time variation in the latitude of the boundary. The midnight boundary index for this period is plotted in Figure 3. In general, it is an excellent indicator of the level of auroral activity. For this storm period the midnight boundary index reached a minimum value of ~38° magnetic latitude (MLAT) late on February 8. One notes that within the general equatorward motion of the oval boundary on February 7 and 8, there was a significant recovery of the midnight boundary index to higher latitudes during a short period late on February 7 and early on February 8.

The change in auroral activity during this contraction can be seen in the F6 white light imagery shown in Figure 4. Before and after the recovery very bright and very wide features occurred in the auroral zone, and the polar cap was dark. By

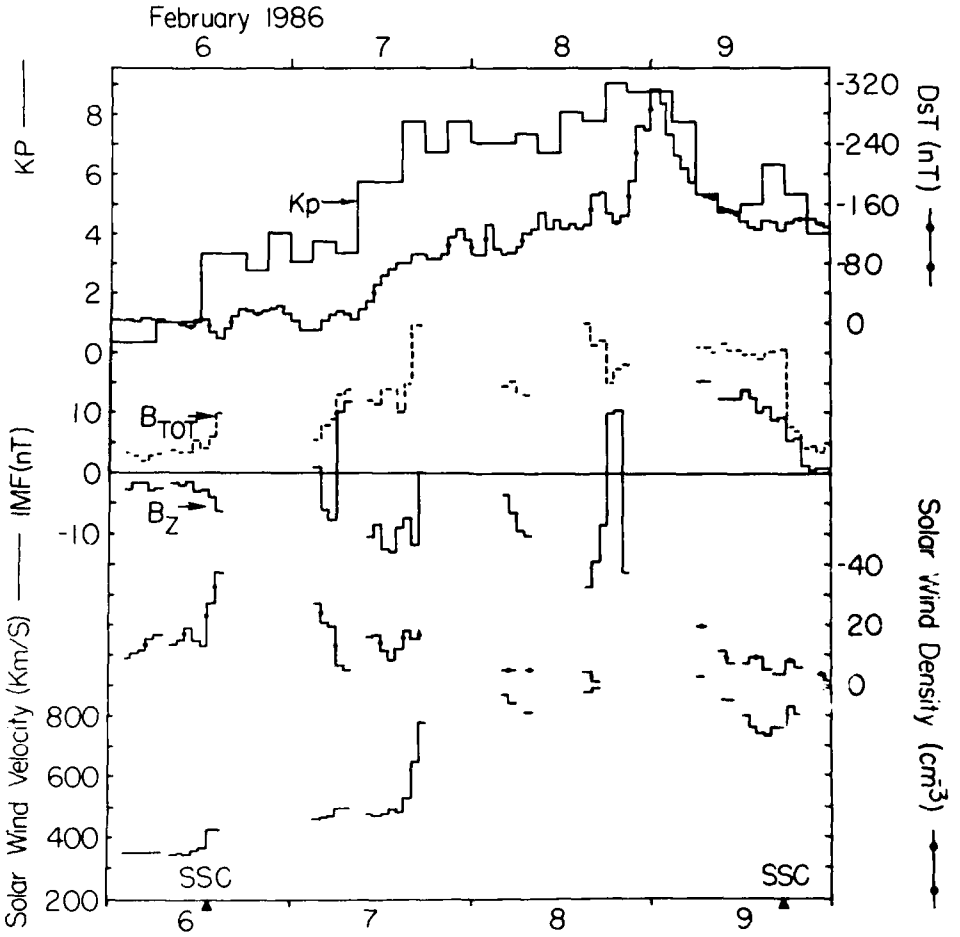

Fig. 2. Indications of the solar-terrestrial environment before, during and after the geomagnetic storm: the K_p and D_{st} indices from standard ground magnetometer stations and the interplanetary magnetic field and solar wind from the IMP 8 satellite. The period from 0130 to 0400 hours UT on February 8, 1986 when there is activity in the polar cap and quiescence in the auroral zone, is the focus of this report.

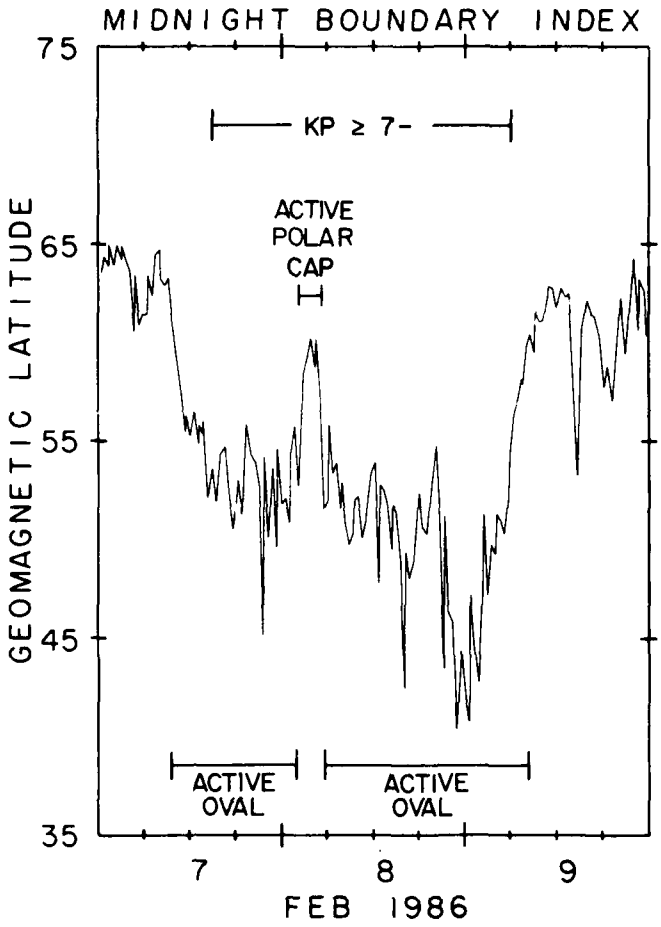

Fig. 3. The auroral boundary index–the equatorward auroral boundary scaled to the midnight meridian–derived from the DMSP particle data during the February 1986 geomagnetic storm. The bar above the data early on February 1986 indicates the period of study when the IMF was probably northward.

contrast, during the recovery, the auroral zone features disappeared, and polar cap arcs are seen in the imagery, albeit dimmer than the auroral arcs before and after this period. This quieting of auroral activity is not seen in the K_p or D_{st} indices. This is probably due to the K_p index's 3-hour granularity, and the D_{st} index's sensitivity to the ring current which does not recover as quickly as the auroral oval. If the AE index of auroral activity were available, it should mirror the recovery seen in the midnight boundary index.

We concentrate in this paper on the period of contraction and re-expansion of the auroral oval on February 8, 1986. In another paper [*Gussenhoven and Mullen*, 1989], we have examined the period between the SSC event and the beginning of major auroral activity on 7 February 1986, as indicated by the K_p and D_{st} indices. Like the period we study in this paper, the IMF was northward in this period, and polar cap arcs were observed. At the same time, however, a solar proton event was in progress, making it possible to compare relativistic electron entry with polar cap arc occurrence. The solar proton event had ended by the time the event discussed here commenced.

The contraction of the auroral oval late on February 7 and early on the February 8, 1986, appears to be in response to the northward turning of the IMF some time between 1700 UT on February 7 and 0200 UT on February 8, 1986. IMP 8, IMF data show that IMF B_z was strongly southward up to at least 1700 UT on February 7 and again after 0500 UT on February 8, 1986. No IMP 8 data exist for the interval from 1700 to 0500 UT. However, between 0200 and 0600 UT on February 8, 1986, the AMPTE IRM spacecraft measured the magnetic field when the spacecraft was in the dawnside magnetosheath. The sign of the B_y and B_z components in the magnetosheath as measured by AMPTE IRM should be comparable to the B_y and B_z components in the un-shocked solar wind, although the magnitude should be larger. These data show that from 0200 to 0406 UT, the B_y and B_z components in the magnetosheath were between +5 and +20 nT and between +30 and +40 nT, respectively, except for a 4 min excursion to $\sim$ +30 and $\sim$ 0 nT, respectively, at 0243 UT. At 0406 UT, B_y and B_z abruptly turned negative, varying between −15 and −30 nT and between 0 and −15 nT, respectively, between 0406 and 0500 UT. Subsequently B_z in the sheath decreased steadily to −30 nT by 0600 UT (H. Lühr, privite communication, 1988), matching closely the trend in the IMP data.

An overview of the changes in the low-altitude, field-aligned current configuration and strength before, during and after the period of boundary contraction is shown in Figure 5. In the figure the ΔB_z component in spacecraft coordinates from the F7 magnetometer (which is approximately equivalent to $\Delta B_{\text{east-west}}$) is plotted for the passes covering this period. Considering the northern auroral zone first, we note that at the start of the interval, large-scale region 1 / region 2 currents occurred with maximum magnetic deflections of $\sim$ 1700 nT. This is four times larger than the maximum deflection observed during a typical ($K_p \sim 5$) disturbed period. Over the next two northern hemisphere passes, the magnitude of the deflections decreased sharply such that by the 0215–0240 UT northern pass where the IMF was clearly northward, no measurable region 1 / region 2 currents were present. Instead the deflections are dominated by small-scale ($L \leq 300$ km or 3° MLAT) field-aligned currents distributed sporadically across the high-latitude region.

As we will show later, weak, longer scale length current regions are still present after the smaller-scale currents are disregarded or filtered out. These relatively weak, longer-scale current regions, however, do not display the signature of the NBZ current system and at best display very weak region 1 / region 2 currents. This behavior is maintained for the next north pole pass. By the 0538–0603 pass, after the southward turning of the IMF, the region 1 / 2 currents are again present.

For the spacecraft magnetometer data over the north pole, the sign of the magnetic deflections due to the region 1 / region 2 currents in the nightside auroral oval reversed between $\sim$2100 UT and $\sim$ 0500 UT. This arises from the shifting of the satellite track in magnetic coordinates such that the orbit intersected the auroral zone westward of the Harang discontinuity prior to $\sim$0000 UT on February 8 and eastward of the discontinuity by 0500 UT.

In the southern high-latitude region, the strength of the nightside region 1 / region 2 currents underwent a similar decrease. In this case the currents were initially weaker since the orbit intersects the auroral zone at earlier evening hours. The NBZ current signature was first apparent in the 0127–0152 UT pass but confined only to a portion of the high-latitude region. By the next southern hemisphere pass (0308–0332 UT) a very prominent NBZ current system extended across the entire high-latitude region. At approximately the same time, the region 1 / region 2 currents in the northern hemisphere were immeasurably small. The positive (sunward) deviation in the NBZ system was as great as $\sim$ 900 nT, and the negative (antisunward) devia-

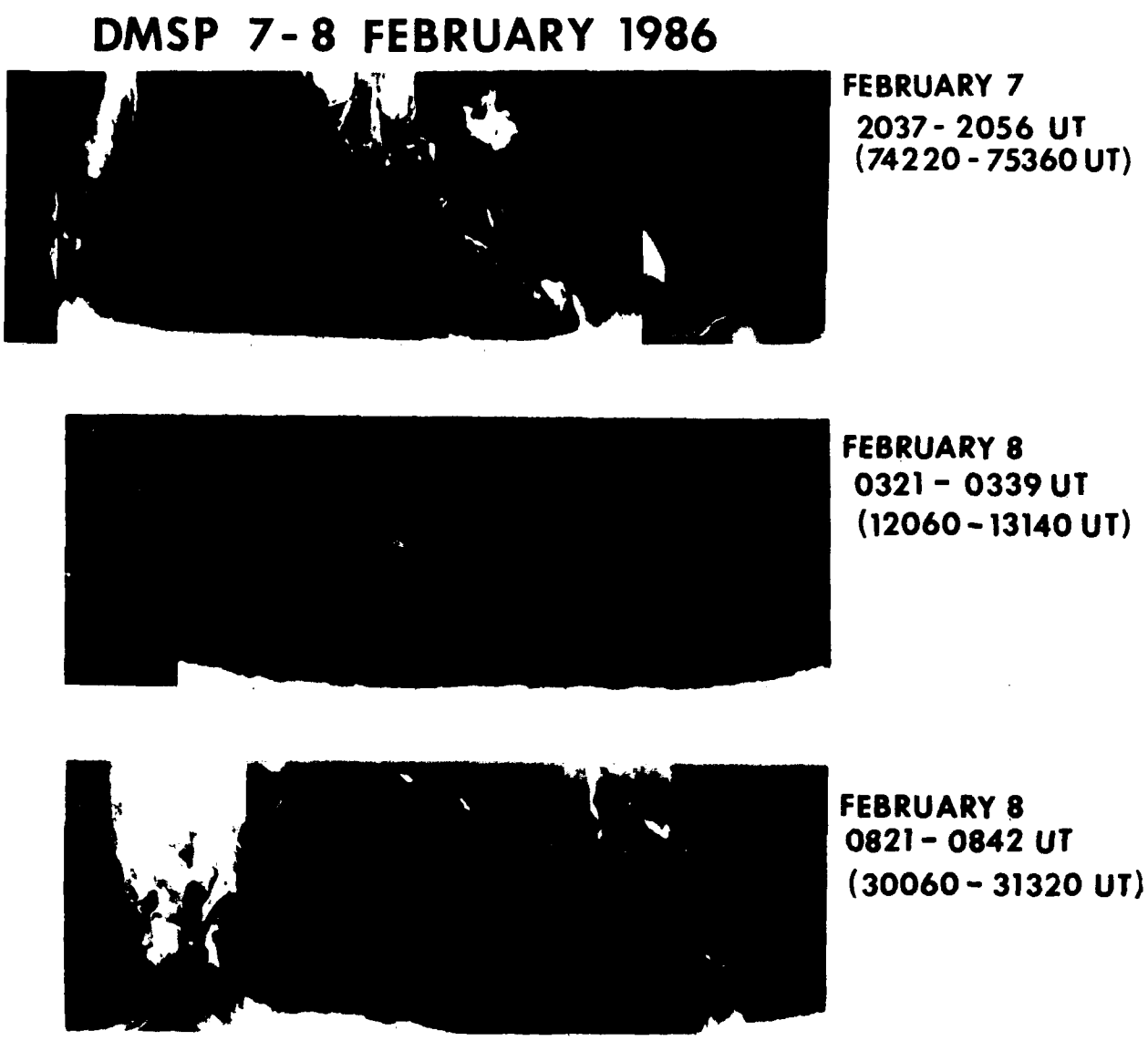

Fig. 4. White light images of auroral emissions across the northern high-latitude regions from DMSP F6 immediately before, during and after the period of polar cap activity and auroral zone quiescence with the storm.

tions were ~600 nT. This is approximately 5 times larger than the typical NBZ system and approximately equal to the largest magnitude for the NBZ magnetic signature reported by *Iijima and Shibaji* [1987]. By the following southern hemisphere pass (0448–0512 UT), approximately 30 min after the southward turning of the IMF observed by AMPTE IRM, the NBZ currents disappeared, and the region 1 / region 2 currents began to reappear.

For the southern passes, the sign of the deviation for the region 1 / region 2 currents on both the dayside and the nightside reversed between the beginning and the end of the interval. Like the northern passes, this resulted from the motion of the DMSP orbit track in the MLT-CGL (corrected geomagnetic latitude) coordinate system. At the beginning of the interval, the region 1 / region 2 currents were encountered postnoon and pre-midnight; by the end of the interval, the intersection was prenoon and postmidnight.

3.2. *Particle Morphology and Variations*

The examination of the particle precipitation patterns and their relationship to the field-aligned current regions during the contraction of the auroral oval is divided into three parts. In the first part we explore the temporal variation of the various regions of high-latitude particle precipitation. In the second part we examine the relationship of these regions to the field-aligned currents. In the third part we characterize the electron and ion spectra within each of the large scale current sheets of the NBZ current system.

General particle morphology: Four high-latitude DMSP passes in the time interval from 0230 to 0340 UT for which the north pole images show the presence of polar cap arcs are used to illustrate the evolution of the electron and ion precipitation pattern during the period of northward IMF. Figures 6 and 7 show data from the F6 satellite and Figures 8 and 9 show data from the F7 satellite. The four passes represent the high-latitude data for one complete orbit for each satellite and encompass the period of the maximum contraction of the electron equatorward boundary, the maximum extent of the boundary plasma region and the maximum NBZ current. Data from the DMSP F6 and F7 satellites (in Figures 6 and 8 and in Figures 7 and 9) were obtained nearly simultaneously in opposite poles.

In each figure, the particle data are plotted in six panels: three each for electrons and ions. In each set of three

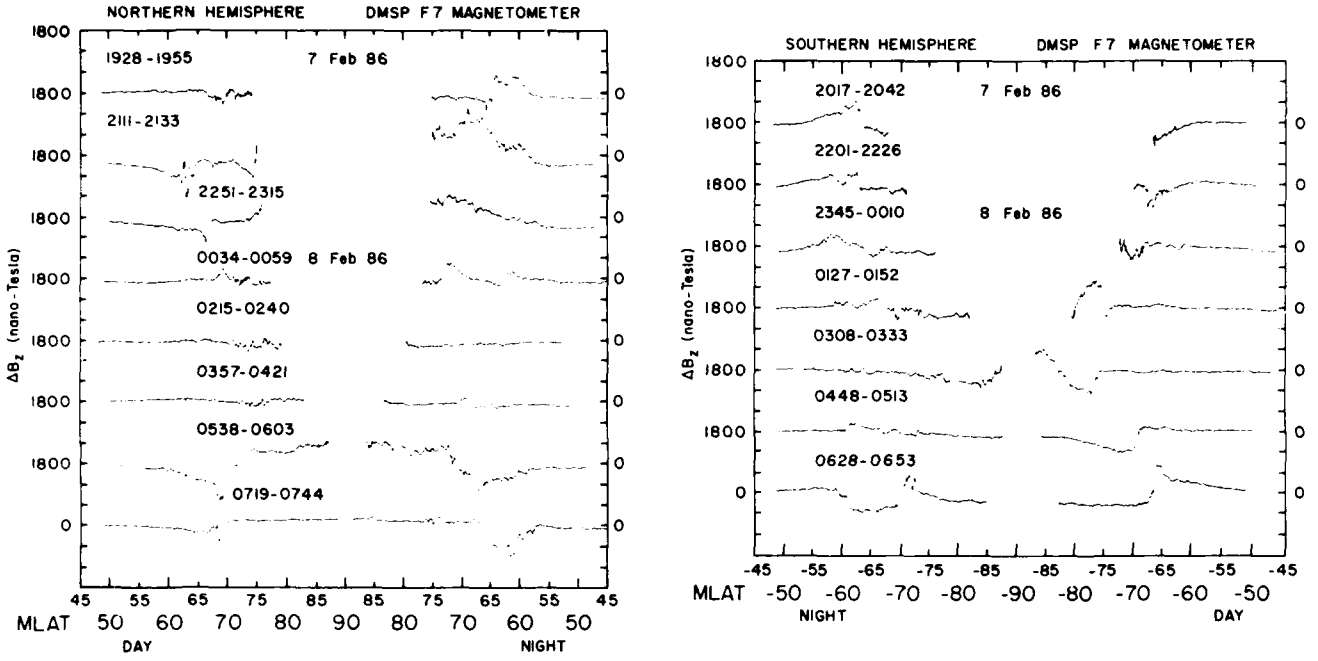

Fig. 5. Cross-track component of the magnetic deflection vectors (ΔB_z) observed by the DMSP F7 satellite as it passed over the northern and southern high-latitude regions before, during and after the period of northward IMF during the geomagnetic storm. The positive z axis is directed to ~1600 hours local time. Positive ΔB_z tends to indicate sunward convection in the southern hemisphere and antisunward convection in the northern hemisphere. The magnetograms are plotted as a function of magnetic latitude; since the satellite does not cross the magnetic pole in these passes, there is a break in the plotting at high latitudes.

panels the average energy: integral energy flux and integral number flux are plotted from top to bottom in units of keV, keV/cm^2 s sr and particles/cm^2 s sr, respectively. The bottom of each figure is annotated with the universal time, and the geomagnetic latitude and local time of the satellite both mapped down the field lines to an altitude of 110 km. The three plasma parameters provide a survey of the variation in the electron and ion precipitation over each pass. They do not, however, fully characterize the plasma. The average energy in particular does not necessarily reflect the particle temperature but rather is affected also by bulk flows in the plasma and field-aligned accelerations. Figures 8 and 9 for F7 have two additional panels which give the horizontal components of the magnetic deflection vectors in spacecraft coordinates.

In the low-altitude precipitating particle data, three distinct regions of plasma precipitation are commonly observed at high latitude: (1) The region of relatively hot plasma populated by particles originating in the central plasma sheet (CPS) [*Winningham et al.*, 1975]. (2) The region of cooler, magnetosheath like plasma mapping to the various magnetospheric boundary plasma regions (BPR) [*Vasyliunas*, 1979]. (3) The region of polar cap (PC) precipitation mapping to the lobes of the geomagnetic tail [*Winningham and Heikkila*, 1974]. In this study we have identified these regions based upon sharp and significant differences in the ion and electron characteristics between the regions. In Fig. 6 to 9, the various regions are labeled, and the boundaries between the regions are denoted by vertical lines. We do not use the term "boundary plasma sheet" because this term was coined [*Winningham et al.*, 1975] to denote the plasma region above and below the plasma sheet in the magnetotail. Here BPR is used to indicate the region at low altitude that maps not only to the boundary plasma sheet but also to the low-latitude boundary layer, the mantle and the cusp/cleft [*Vasyliunas*, 1979].

For the polar cap region (PC) we note that during periods of polar cap arc activity the boundaries and extent of this region can be ambiguous due to the slow variation in the level of particle precipitation between the BPR and PC and the similarity in spectral characteristics for the particles in the two regions. In fact, it may be the case that all the precipitating particles in the tail lobe originate in the magnetospheric boundaries. Our definition of the polar cap will be "the high-latitude region where the lowest baseline levels of electron precipitation are observed." This definition implies nothing about whether the field lines in this region are open or closed.

We use the pass in Figure 6 to illustrate the characteristics of the various plasma regions and the criteria used to select the boundaries of these regions. The equatorward boundary of the CPS is taken as the equatorward boundary of auroral ion or electron precipitation determined using the criteria of *Gussenhoven et al.* [1983, 1987]. For this pass the electron (ion) boundaries are chosen at −63.0° (−60.6°) and −53.4° (−61.1°) on the eveningside and morningside, respectively. The CPS itself is identified as the region of approximately thermal, multikilovolt electron and ion precipitation whose characteristics vary slowly and smoothly with latitude. Common characteristics of the CPS that were found in this pass are a dawn-dusk offset between the electron and ion CPS equatorward boundaries and a higher (lower) peak average energy for ions (electrons) on the eveningside as compared to the morningside of the oval.

The boundary between the CPS and the BPR is chosen where the average energy of the electrons drops abruptly from values of one to several keV to values of approximately 100 eV. This selection criterion is similar to that used by *Makita and Meng* [1984] and *Holzer et al.* [1986]. The boundaries chosen in this manner are coincident with a leveling off of the ion average energy at values of a few keV. For the pass in Figure 6 the evening (morning) CPS/BPR

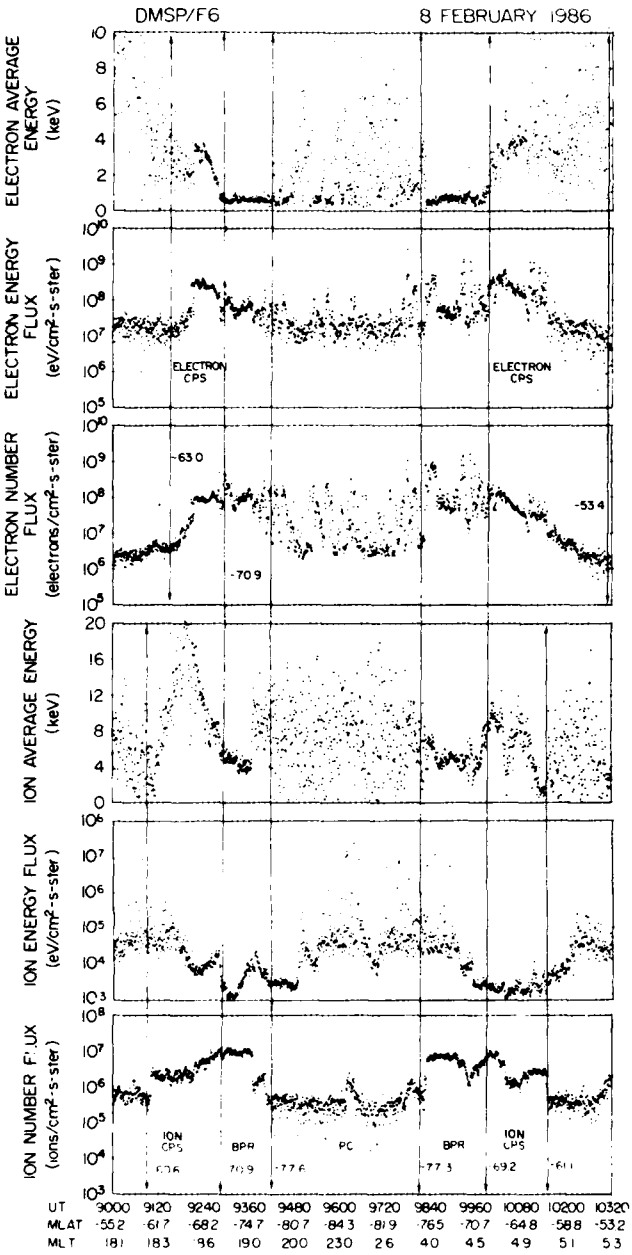

Fig. 6. Ion and electron data obtained from the southern polar pass of the DMSP F6 satellite from 9000 s (0230 hours) to 10320 s (0252 hours) UT during the northward IMF period.

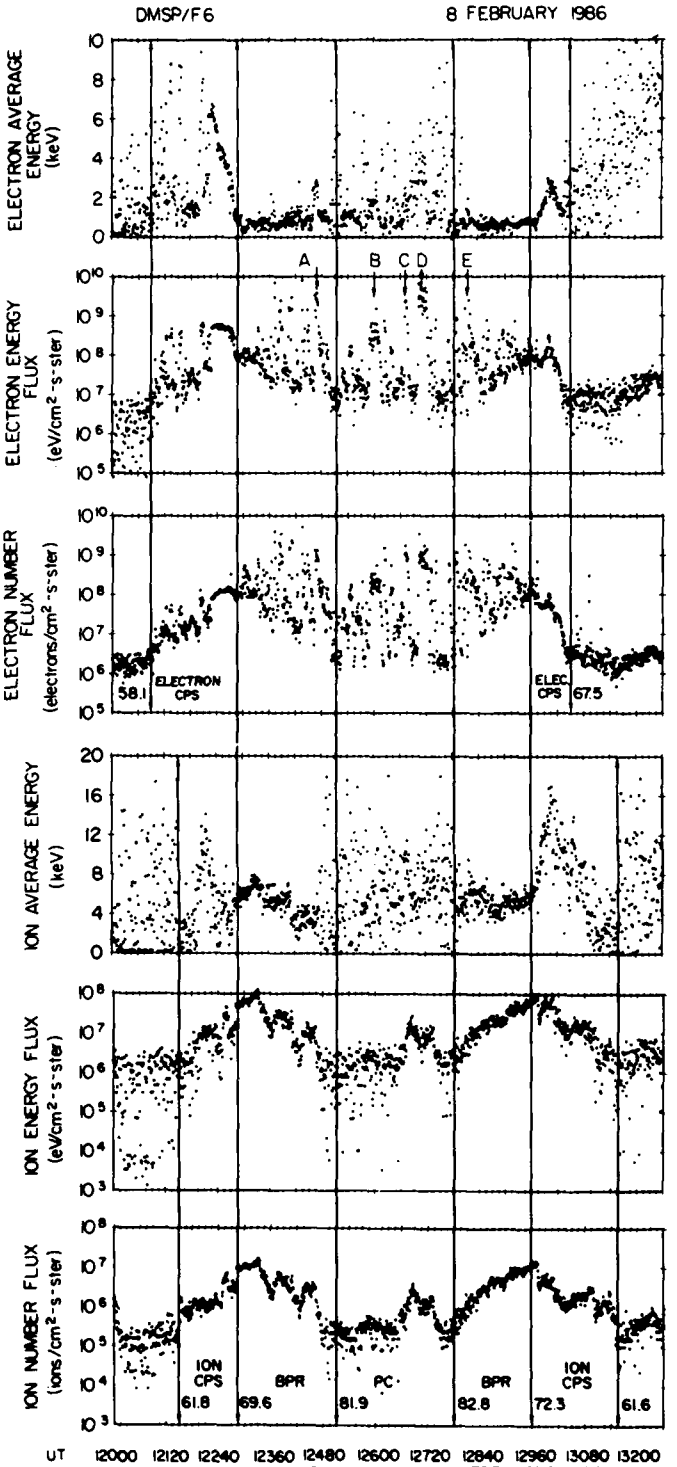

Fig. 7. Ion and electron data obtained from the northern polar pass of the DMSP F6 satellite from 12000 s (0320 hours) to 13260 s (0341 hours) UT during the northward IMF period. Five enhancements of electron precipitation related to visible arcs are labeled with letters A through E.

boundary is chosen at -70.9° (-69.2°) CGL. In the BPR, on both sides of the oval, the electron and ion average energies remained approximately constant and at low values relative to the CPS. The electron flux in the BPR remained relatively high but became more variable with small spatial and/or temporal structures throughout much of the region. The fluctuations occurred above a baseline value in the integral number flux. The baseline of the integral number flux decreased with increasing latitude in the BPR and eventually fell to a level typically associated with the polar rain, i.e. integral number flux < 10^7 electrons/cm^2 s sr and average energy of ~100 eV [*Winningham and Heikkila*, 1974; *Riehl and Hardy*, 1986].

The boundary between the BPR and PC is chosen as the lowest latitude at which the baseline level of the integral number flux of the polar rain occurs. For the pass in Figure 6, using a baseline level of approximately 5 × 10^6 electrons/cm^2 s sr, the BPR/PC boundary is set at -77.6° and -77.3° on the eveningside and morningside of the oval, respectively. These boundaries of the electron fluxes are at approximately the same latitude where the level of ion inte-

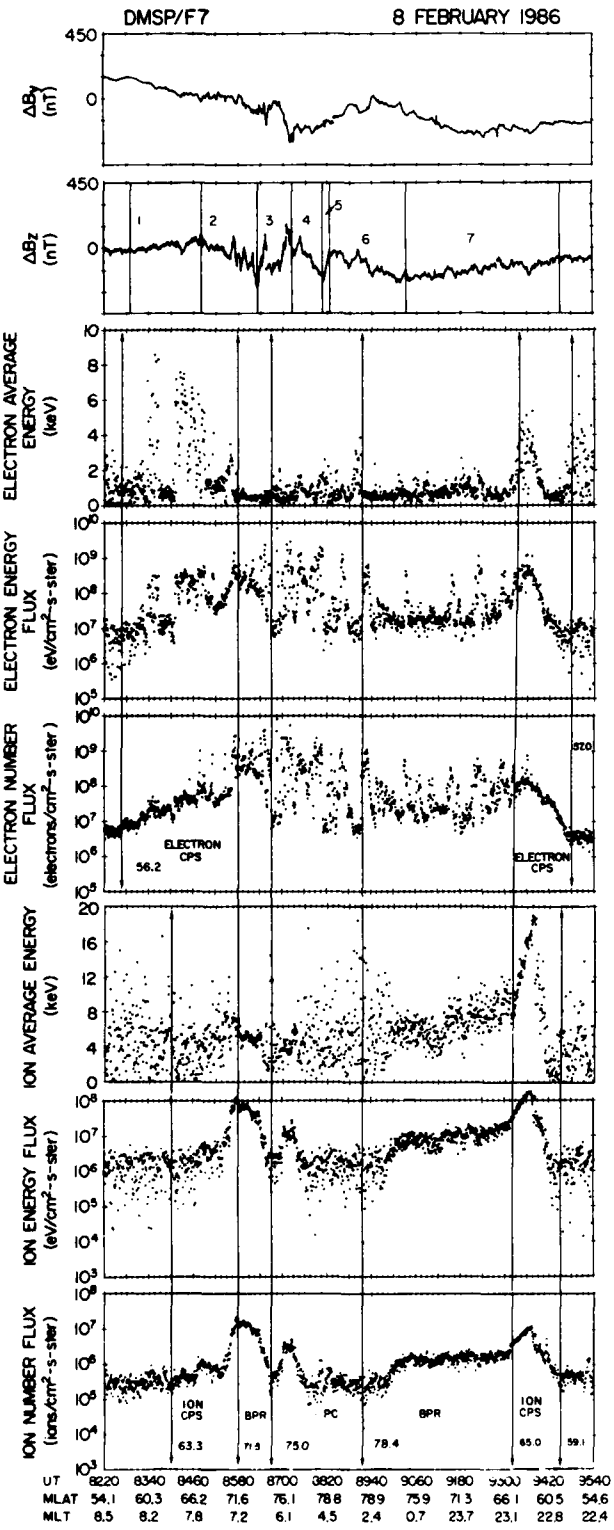

Fig. 8. Ion and electron data and magnetic field data obtained from the northern polar pass of the DMSP F7 satellite from 8220 s (0217 hours) to 9540 s (0239 hours) UT during the northward IMF period.

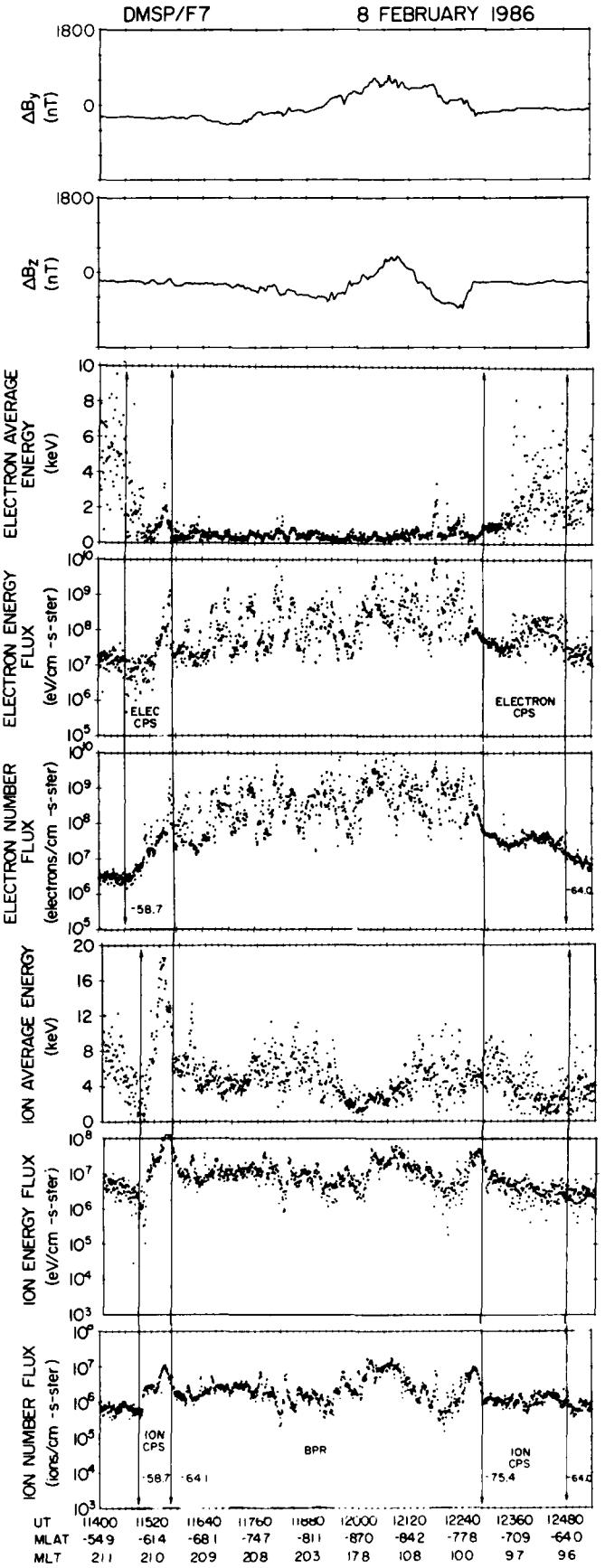

Fig. 9. Ion and electron data and magnetic field data obtained from the southern polar pass of the DMSP F7 satellite from 11400 s (0310 hours) to 12540 s (0329 hours) UT during the northward IMF period. The "W" shape of the ΔB_z trace is the signature of the NBZ current system.

gral number flux and energy flux changed significantly. As has been shown previously for electrons [*Hardy et al.*, 1982], the intensity of the baseline precipitation is the principal distinction between the BPR and PC. The spectral shapes for electrons in the two regions are approximately the same. In the PC the scatter in the average energy, calculated by

dividing the energy flux by the particle flux obtained from 1 s of data and displayed in Figures 6 through 9, is a result of low count rate statistics, and is not representative of the true characteristics of the particle population.

In the manner discussed above, boundaries were selected for all passes in the interval 0050 to 0550 UT on February 8, 1986. The general behavior for the boundaries as determined from these passes is as follows. The equatorward boundaries contracted by more than 10° over several hours and then sharply expanded (see Figure 3). The BPR/PC boundary also advanced dramatically poleward and then receded. For the same period the CPS/BPR boundary remained relatively stationary. As a result in the period of polar cap activity the latitudinal width of the CPS shrank significantly as the BPR width expanded to engulf most, if not all, of the polar region. This is similar to the results of *Makita and Meng* [1984].

These changes are clearly illustrated in Figures 6 through 9. For the two F6 satellite passes, the morningside (eveningside) electron boundaries contracted from −53.4° (−63.0°) to 58.1° (67.5°) within the 50 min between the two passes. For the F7 satellite passes, the contraction on the morningside (eveningside) of the oval was from 56.2° (57.0°) to −64.0° (−58.7°). Although the contraction was seen at all local times, the smallest CPS width occurred for the F7 pass closest to local midnight and at the end of the northward IMF period.

For these two orbits the latitude of the CPS/BPR boundary was relatively constant and showed no consistent pattern of equatorward or poleward motion. On the eveningside (morningside) of the oval, this boundary, for the F6 passes, moved from −69.2° (−70.9°) to 69.6° (72.3°). For the F7 passes, the motion on the eveningside (morningside) was from 71.5° (65.0°) to −75.4° (−64.1°). The electron and ion characteristics within the BPR were approximately independent of the local time or pole sampled. The CPS/BPR boundaries for electrons and ions are in good agreement.

The poleward boundary of the BPR moved strongly poleward in these passes. For the F6 passes, the BPR/PC boundary on both the eveningside and morningside of the oval moved from −77° to 82°. For the first F7 pass, the BPR/PC boundary on the morningside (eveningside) was at a latitude of 75.0° (78.4°). For the second F7 pass, the baseline level of electron and ion precipitation never drops to the level of the polar rain. We interpret this as the BPR having extended on both the morningside and the eveningside of the oval up to the maximum latitude traversed by the satellite, −87.1°. If the PC region contracted symmetrically with respect to the magnetic pole, this implies almost no PC region was present. Alternately, if the PC region contracted in a highly asymmetric manner, then it was probably confined to the early morning sector.

We summarize these boundary variations by plotting in Figures 10 and 11 the variation in the width of the CPS and BPR respectively before, during, and after the polar cap arc period. The only effort to remove any local time effect has been to plot the morning and evening widths separately. On the morningside the CPS width was initially 18°, decreased to a minimum of 7°, and then recovered slightly. On the eveningside the decrease was much steeper, from ∼23° to ∼12° in 30 min. Its minimum of 4° was reached just prior to the southward turning of the IMF, after which it recovered to approximately 10°.

For the BPR, the morningside width was initially ∼14° with the BPR extending to a latitude of ∼85° in both poles. The width first contracted to approximately 7° and then expanded to a maximum of ∼20° just prior to the southward turning. For IMF southward, the widths contracted sharply. The evening variation is much clearer. No BPR was observed at the beginning or end of the interval; i.e., for these

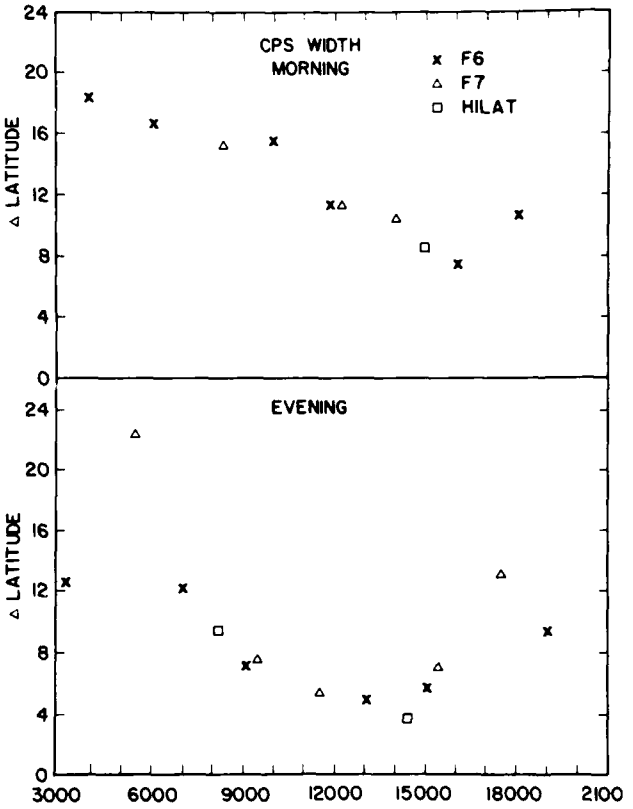

Fig. 10. Width of the central plasma sheet (CPS) region traversed by the DMSP F6, DMSP F7 and HILAT satellites in the morning and evening sectors.

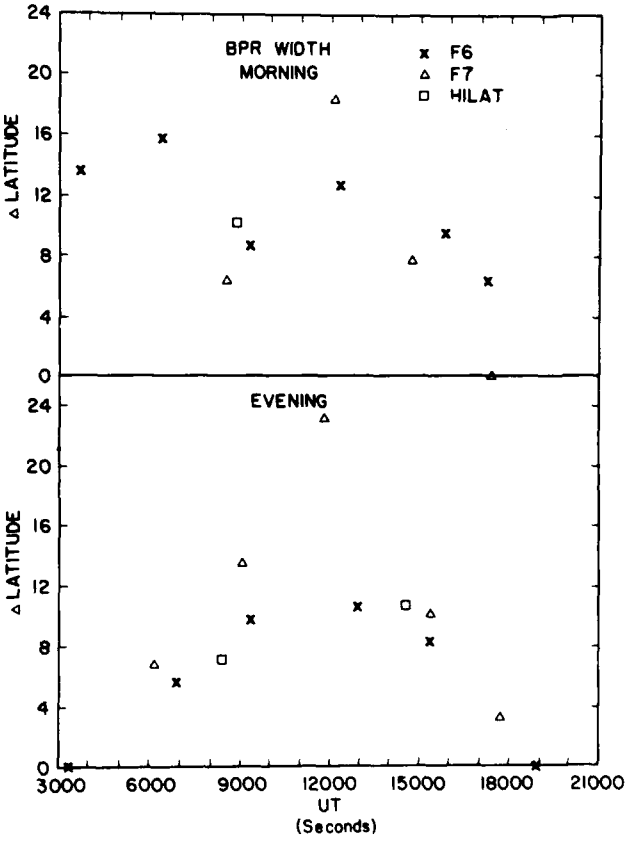

Fig. 11. Width of the boundary plasma region (BPR) region traversed by F6, F7 and HILAT in the morning and evening sectors.

passes the electron and ion flux at the poleward boundary of the CPS dropped directly to the level of the polar rain. As the electron equatorward boundary contracted, the BPR appeared on the eveningside and rapidly expanded, reaching a maximum extent of at least 23°. At the maximum extent, the boundary region penetrated to the maximum latitude reached by the satellite, 87.1° CGL in the southern (summer) hemisphere. With the southward turning of the IMF, the region contracted. For both evening and morning sides of the auroral zone, the expansion and contraction of the various regions were approximately the same in both poles.

Confirmation that the changes in the boundaries and extent of the CPS, BPR and PC are occurring simultaneously in both poles is provided by the HILAT data. Approximately 15 min before the F6 pass shown in Figure 6, the HILAT satellite passed over the opposite pole. As shown in Figure 1, the two passes were approximately coplanar. For these two passes the electron equatorward boundary, the CPS/BPR boundaries, and the BPR/PC boundaries for HILAT and DMSP F6 were all within a degree or two of each other.

For all four passes shown in Figures 6–9, small-scale fluctuations in the electron integral number and energy flux occurred throughout much of the BPR and PC. The ion precipitation showed no such structure. The spatial scale and intensity of the small-scale structures in the electrons is much the same in the BPR and PC as has been reported previously [*Hardy et al.*, 1982]. In the polar cap, we identify these structures as polar showers or polar squalls [*Winningham and Heikkila*, 1974] associated with Sun-aligned, polar cap arcs.

The optical characteristics of these polar cap arcs are illustrated in the DMSP F6 image (Plate 1) obtained during the northern polar pass starting at 0320 UT. (Plate 1 is shown here in black and white. The color version can be found in the separate color section in this issue.) The figure has been created from the original DMSP image (shown in Figure 4) by using a microdensitometer to digitize the light intensities on the original image. These intensities were then color coded with intensity increasing from blue to red to white. In Plate 1 noon is toward the bottom and midnight towards the top. Here we can see that there were no well-defined regions of the cap in which arcs or arc patches were absent. Sun-aligned arcs extended both across portions of the cap or entirely across the area of the cap imaged. In the image and in Figure 7, letters are used to mark the arcs and the corresponding increases in the integral energy and number flux with which they are associated. A number of the arcs are seen to lie clearly in the boundary plasma region as we have identified it, and several are clearly in the polar cap embedded in regions of precipitation at polar rain levels.

In addition to the above characteristics, Figures 8 and 9 also illustrate that the variations in the extent of the high-latitude plasma regions occur in tandem with changes in the field-aligned current systems. The shrinking of the latitudinal width of the CPS was coincident with the disappearance of the auroral zone region 1 / region 2 currents. In addition, the expansion of the boundary plasma region to higher latitudes occurred simultaneously with the appearance of the NBZ current system in the south pole. This is particularly clear for the south pole F7 pass shown in Figure 9 where the BPR extended approximately to the pole. For this pass the NBZ current system clearly collocates with the BPR, i.e. the NBZ current system is not in the polar cap region as we define the PC from the precipitating electrons and ions.

For the preceding north pole pass for F7 (Figure 8), there are numerous, small-scale pairs of field-aligned currents. On a larger spatial scale, however, we have identified seven current regions. In Figure 8 the boundaries of these regions are marked by vertical lines and the seven current regions

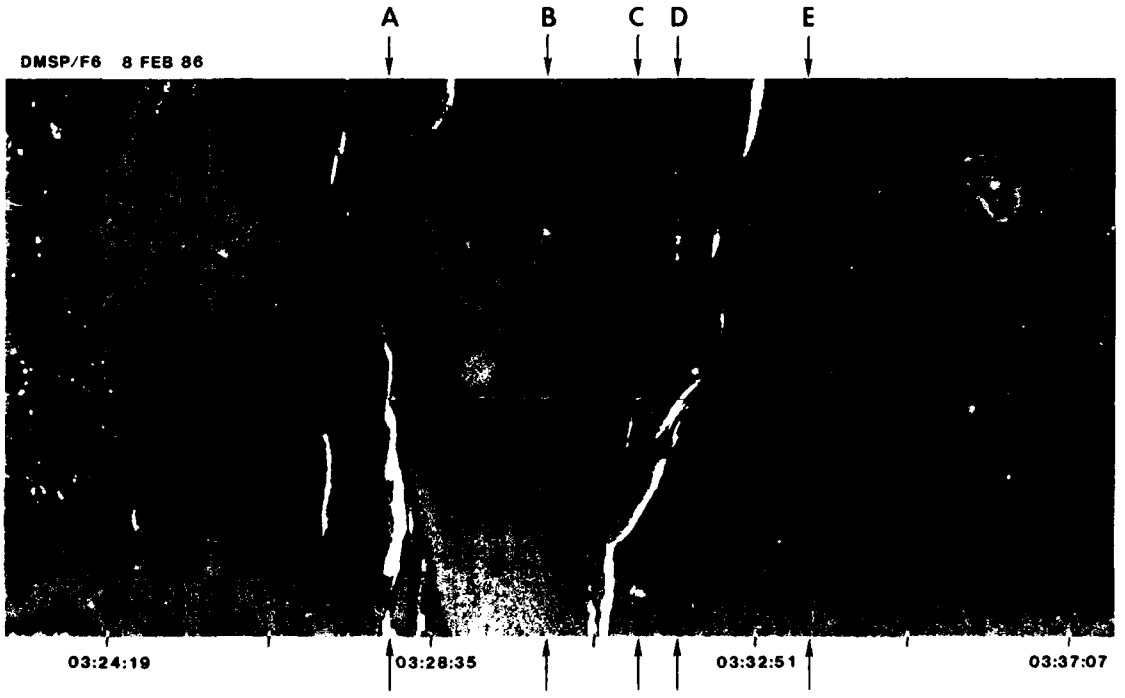

Plate 1 (*Rich et al.*). False color reproduction of DMSP F6 white light imagery data obtained during the 0320–0341 UT pass through the northern (winter) high-latitude region. Numerous Sun-aligned, polar cap arcs are visible at very high latitudes. The satellite passed from left to right, and the imager scan lines are from the bottom to the top of the figure. The nadir look position has been marked with reverse color. Five visible arcs related to the electron flux enhancements marked in Figure 7 are labeled on the edge of the image with letters A through E. The color version of this figure can be found in the separate color section in this issue.

labeled 1 through 7. The intensity of these currents is much smaller than the intensity of those seen in either the immediately preceding or subsequent south pole passes but clearly reflects significant deviations from the baseline. There are two points of note in regard to these spatially larger current regions. First, except for the two equatorward boundaries, none of the current boundaries are coincident with particle boundaries. Second, and more importantly, the currents do not display the NBZ pattern. Since the two south pole passes that bracket this pass in time do display the NBZ current system, this implies a difference between the poles in the large scale currents observed. This point will be considered in more detail in the discussion section. In addition, one should note that in the F7 passes shown, the normal region 1 / region 2 current system was small or absent.

In the F7 passes in both poles, the small-scale structures in the electrons producing the Sun-aligned arcs are also associated with the small-scale structures in the magnetogram indicating the presence of field-aligned currents. Like the small-scale electron structures, there was no difference between the BPR and PC in the intensity or latitudinal extent of these small-scale field-aligned currents. In the F7 south and north pole passes, these small-scale field-aligned currents were observed within large-scale regions of both upward and downward field-aligned current and were observed over the entire high-latitude region.

Field-aligned current characteristics during the NBZ passes: Next, we analyze in more detail two south pole passes of DMSP F7 (0127–0152 UT and 0308–0332 UT) during which large-scale NBZ currents occurred. Data from the latter pass were shown in Figure 9. The detailed data are shown in Plates 2 and 3 where color spectrograms of the electron and ion data are plotted with line plots of the two transverse components of the ΔB vector. (Plates 2 and 3 are shown here in black and white. The color versions can be found in the separate color section in this issue.)

In the first NBZ pass (Plate 2), the signature of the NBZ current is not observed to extend across the entire polar cap, nor does the magnetogram exhibit the symmetric "W" shape which is often associated with the system. There are, however, four current sheets in the correct sense for the NBZ system: the three current sheets toward the dayside encountered in the interval from 0140 to 0143 UT and a fourth, more spatially extended region towards the nightside encountered from approximately 0132:30 to 0136:00 UT. In the color spectrogram vertical lines are used to mark the boundaries of the four current regions. The boundaries were chosen at the point where the slope of the ΔB_y component changed sign. There is a region of sunward convection associated with the current on the dayside and the color spectrogram also shows that the region of sunward convection was populated by the cool electrons and ions we associated with the BPR. On this pass, there was a small but measurable auroral region 1/ region 2 current system observed on the nightside, but not on the dayside.

During the second NBZ pass (Plate 3), the classic "W" shape is clearly seen in the magnetogram. In the figure we mark the four current regions with roman numerals I to IV (arabic numbers 1 and 2 are reserved for the auroral zone currents). In this case, the NBZ system extended across

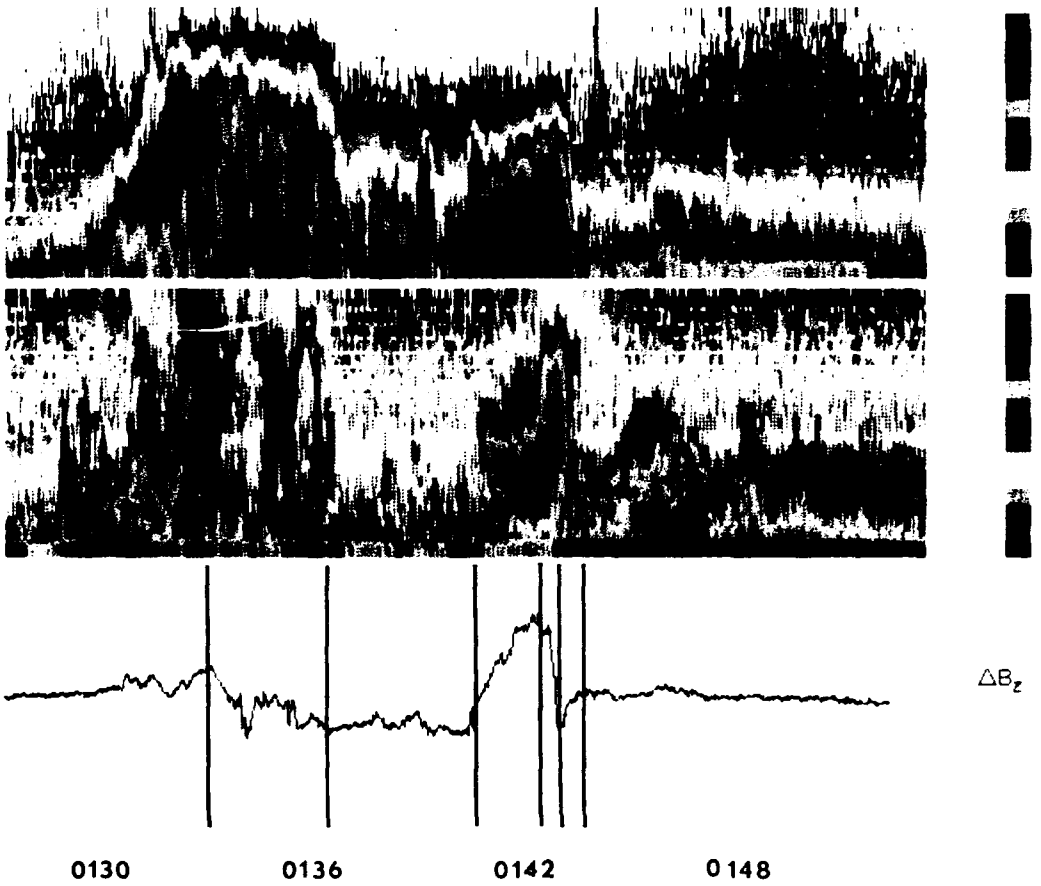

Plate 2 [*Rich et al.*]. DMSP F7 0127–0152 UT: Horizontal components of magnetic deflection (bottom panel) and spectrogram (top and middle panels) showing the distribution of electron and ion flux (color coded) versus energy (vertical axis) versus time (horizontal axis). The boundaries for the CPS, BPR and PC regions of particle precipitation are indicated with vertical lines. The partial NBZ current (0140–0143 UT) occurred entirely within the BPR. The color version of this figure can be found in the separate color section in this issue.

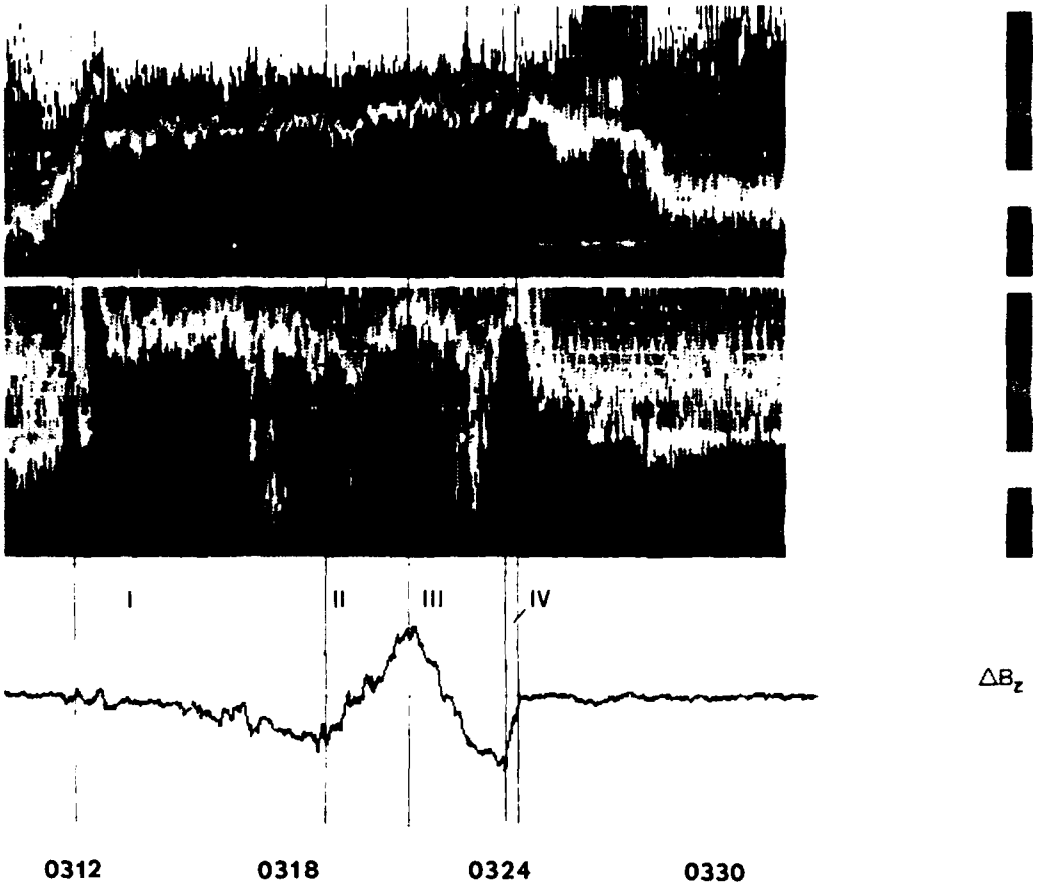

Plate 3 [*Rich et al.*]. DMSP F7 0308–0322 UT: Same format as Plate 2. The boundaries between the four NBZ current sheets or regions are indicated with vertical lines and the regions are denoted with roman numerals. The color version of this figure can be found in the separate color section in this issue.

the entire polar region traversed by the DMSP F7 satellite. Since there were no noticeable auroral oval currents, we selected the beginning of region I where the ΔB_z component first deviated from the baseline, 0312 UT (-60.5° CGL and 21.0 hours MLT). The next three boundaries were chosen at the reversals of the slope of ΔB_z - 0319:00 hours (11940 s) UT, 0321:20 hours (12080 s) UT and 0324:15 hours (12255 s) UT. The last boundary was chosen where the ΔB_z component returns to the baseline: 0324:40 hours (12280 s) UT. The color spectrogram shows that large fluxes of electrons and ions populate all of the current regions. The detailed characteristics of these particles are given in the next section.

In Figure 12 the ΔB vectors for the two NBZ passes are shown at 12-s intervals in magnetic coordinates along the satellite trajectory passes. For the first pass, the magnitude of the ΔB vector goes nearly to zero as the vector reverses direction from sunward to antisunward at the poleward boundary of the nightside auroral zone. This is the typical signature of a quasi-infinitely long current sheet. By contrast the vectors at high latitudes on the dayside for both passes do not abruptly change direction or magnitude between the NBZ current regions. Rather the vector rotates from one orientation to the next with minor changes in magnitude. This rotation indicates that the width is comparable to the length of current regions II and III. We estimate the ratio of the length to width of the polar current region to be 1 to 7 or less, and thus the infinite current sheet approximation is not an accurate description of these current regions.

Particle characteristics during the NBZ passes: In this section we examine the electron and ion spectral characteristics in the NBZ current regions. We first note the high variability in the intensity of the electron precipitation. During the second NBZ pass of DMSP F7 (Figure 9), the electron number flux in the BPR varied from $\sim 3\times10^7$ to $\sim 10^{10}$ electrons/cm^2 s sr and the integral energy flux from $\sim 10^7$ to $\sim 7\times10^9$ kev/cm^2 s sr (1.6×10^{-2} to 11.3 ergs/cm^2 s sr). Variations by a factor of 5 in both the integral number flux and integral energy flux occurred on time scales down to 2 s. Across the entire region, there were numerous enhancements that exceeded 3×10^8 keV/cm^2 s sr. *Hardy et al.* [1982] have shown that enhancement at this level will produce visual features in the DMSP imagery. No DMSP image is available from this pass since the south pole at this time was in sunlight. Nonetheless, these enhancements suggest the presence of as many as 15 Sun-aligned arcs across the cap.

In several cases, the particle enhancements are associated with small-scale upward currents from Sun-aligned current sheets, as would be expected for polar cap arcs. In other cases, the indication of an associated upward current is ambiguous. In these cases, significant spatial and temporal gradients of the field-aligned currents probably affect the magnetogram signature.

Despite the high variability of the electrons, detailed examination of the electron spectra shows that there were only two types of electron precipitation present. The two types are illustrated in Figures 13 and 14 where, in each, the logarithm of the distribution function of the electrons at five

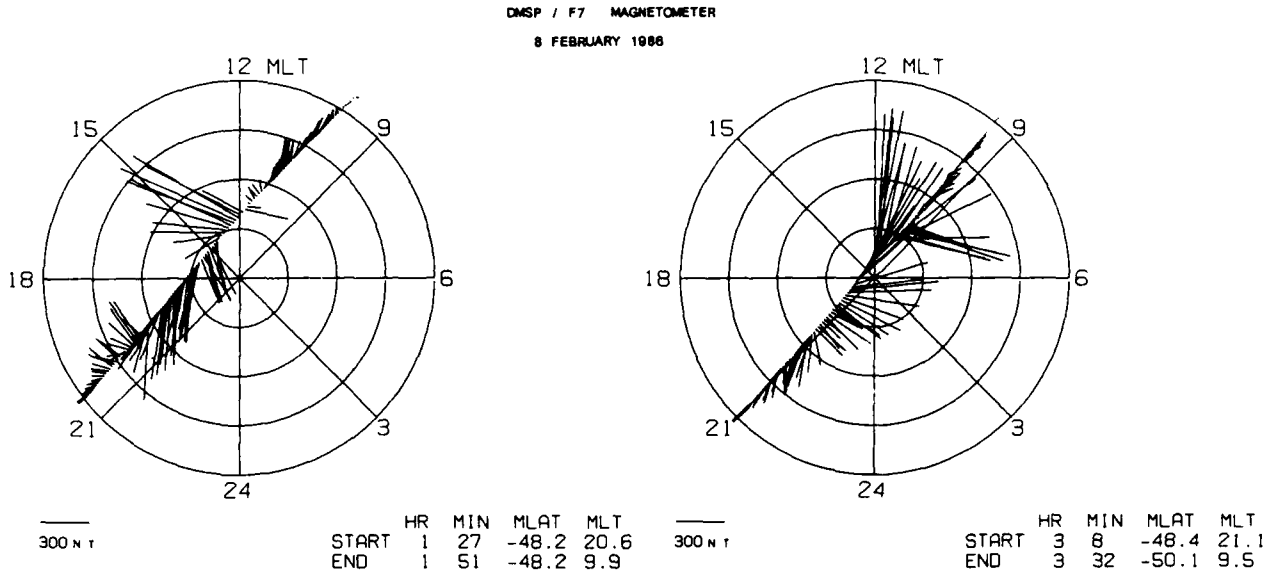

Fig. 12. Horizontal components of DMSP F7 magnetic field deflections during the southern hemisphere passes shown as vectors on a polar projection in geomagnetic coordinates. The base of each vectors is placed at the satellite location.

points across the cap is plotted versus energy on a linear scale. The electron distributions were chosen such that there is at least one representative distribution from each of the four current regions. In Figure 13, the spectra were exterior to any of the structured enhancements within the pass, i.e., when the electron flux was close to the baseline level of approximately 3×10^7 electrons/cm^2 s sr observed across the high-latitude region. In Fig. 14, the spectra were interior to the enhancements. The spectra were obtained at latitudes as high as 85.1°.

In Figure 13, the electron spectra, at energies of 70 eV or less, display a weak peak that we associate with a small-magnitude, field-aligned potential acting on the particles. For energies greater than this peak up to approximately 1 keV, the distribution function is well approximated by a straight line indicating a thermal electron distribution. For energies greater than 1 keV there are indications of a weak high-energy tail to the distribution. Straight lines in the figures show the results of a linear regression fit to the data from the peak to approximately 1 keV. The derived pa-

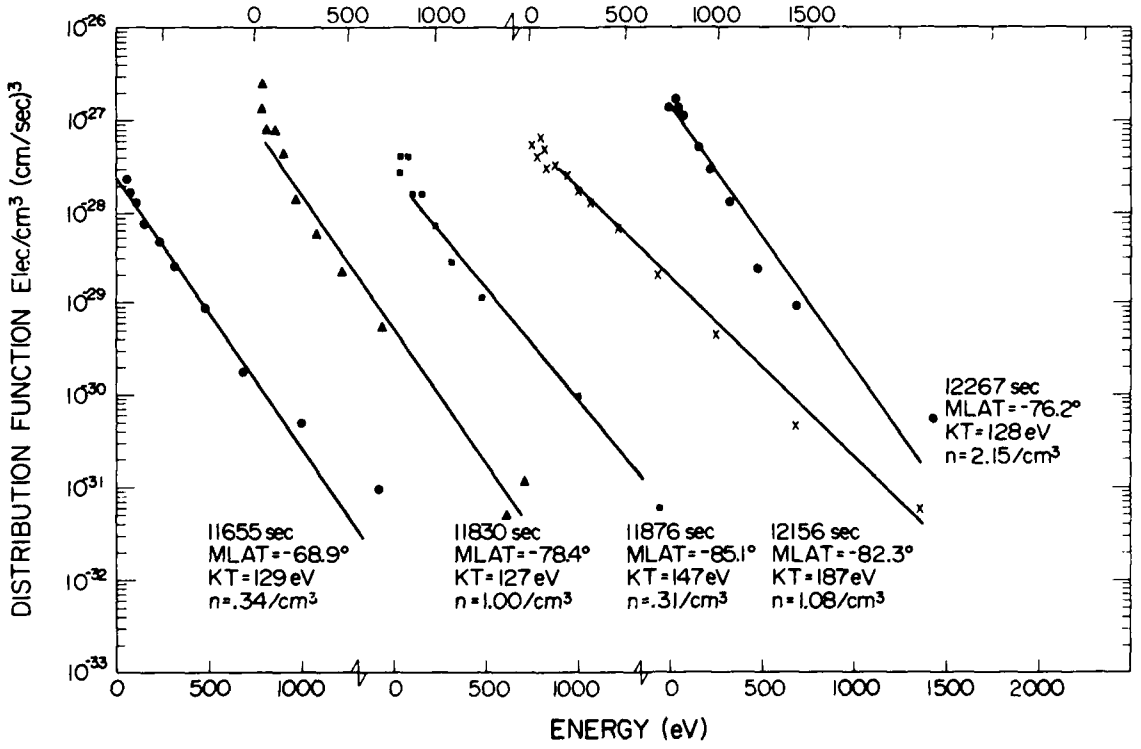

Fig. 13. Distribution functions for selected electron spectra observed in the NBZ current regions. These spectra are from a BPR electron population without acceleration.

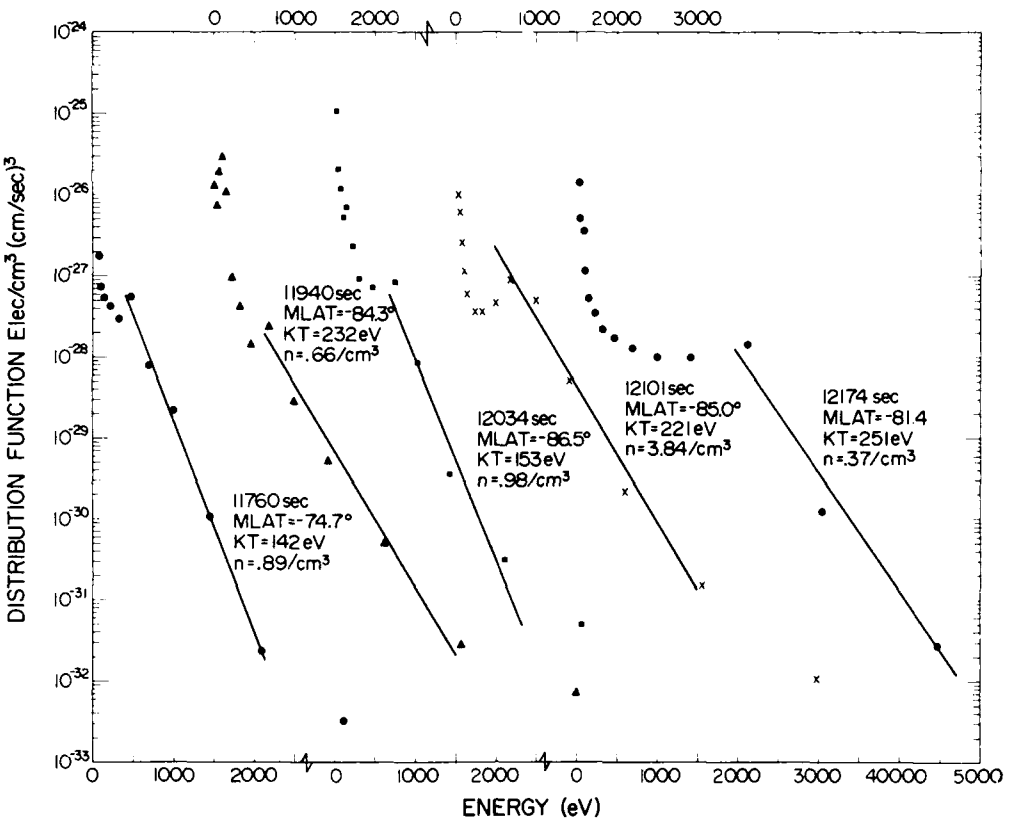

Fig. 14. Distribution functions for selected electron spectra observed in the NBZ current regions. These spectra are from a BPR electron population with an acceleration.

rameters are listed next to each spectrum. The density was determined by shifting the distribution function in energy by the level of the field-aligned potential inferred from the spectrum. The temperatures from the five distributions are similar, ranging from 127 to 187 eV, with densities from 0.31 to 2.15/cm^3. These values are significantly greater than the average temperature of the polar rain of 80 eV and the mean density of the polar rain of 0.055/cm^3 [*Riehl and Hardy*, 1986]. Also, the temperature is significantly less than typical plasma sheet spectra, while the density is slightly less.

The large degree of structure in the electrons results from spatially and/or temporally varying regions of field-aligned acceleration across the high-latitude region. The level of the fluctuations results primarily from the magnitude of the field-aligned potential and not from major changes in the parent population experiencing the acceleration. This is shown in Figure 14. All the spectra in the figure exhibit a peak at energies ranging from approximately 460 to 2100 eV. As in Figure 13, we interpret these peaks as the result of field-aligned potentials. A linear regression was performed on the points beyond the peak to determine the temperature and number density of the unaccelerated electrons. For energies well above the peak there are indications of a high-energy tail. These points were not included in the fit. The derived number densities range from 0.37/cm^3 to 3.84/cm^3 with all but one of the examples less than 1.0/cm^3. The temperatures range from 142 to 251 eV. The densities agree closely with those in Figure 13, while the temperatures are somewhat higher. The slightly higher temperatures may reflect heating of the electrons in the acceleration process [*Lin and Hoffman*, 1982].

The general picture derived from the electron measurements is that, during the NBZ passes through the BPR, a fairly homogeneous region of cold and moderately dense electrons extended up to a latitude of at least -87.1°; the highest latitude observed. The temperature and density of these electrons were well above the average level of the polar rain and were consistent with the electron characteristics in the boundary plasma region. The high degree of structure across the pass arose from the acceleration and slight heating of these electrons by temporally and/or spatially varying field-aligned potentials. The observation of such cold electrons in the polar cap and their association with Sun-aligned arcs has been previously reported [*Burke et al.*, 1982; *Hardy et al.*, 1982].

As for the precipitating electrons, the ions displayed similar spectral characteristics throughout the BPR for this pass. Representative spectra from each of the four NBZ current regions are plotted in Figures 15 through 18 where they have been chi-square fit to a series of flowing and nonflowing Maxwellian distributions. The figures illustrate that the ion spectrum was typically peaked at energies from 100 eV to 3 keV. For energies near the peak the shape of the ion spectrum is consistent with a flowing (V_b = 200 to 600 km/s), cool (kT = 30 eV to 400 eV) and relatively low-density (10^{-2} to 10^{-3} ions/cm^3) ion population. At energies well above the peak the spectrum most often exhibited a high-energy tail. This tail is reasonably fitted to a thermal distribution (kT = 1 to 4 keV) with relatively high number densities compared to the low-energy flowing component (n = 0.1 to 1.0 ions/cm^3). The high-energy tail thus carried the majority of the number and energy density of the precipitating ions. In a minority of the spectra instead of a high energy tail there was a secondary peak consistent with a second, higher-velocity, flowing ion population. The above characteristics are similar to those reported for magnetosheath and boundary layer ions and are inconsistent with a plasma sheet origin for these particles [*Eastman et al.*, 1985].

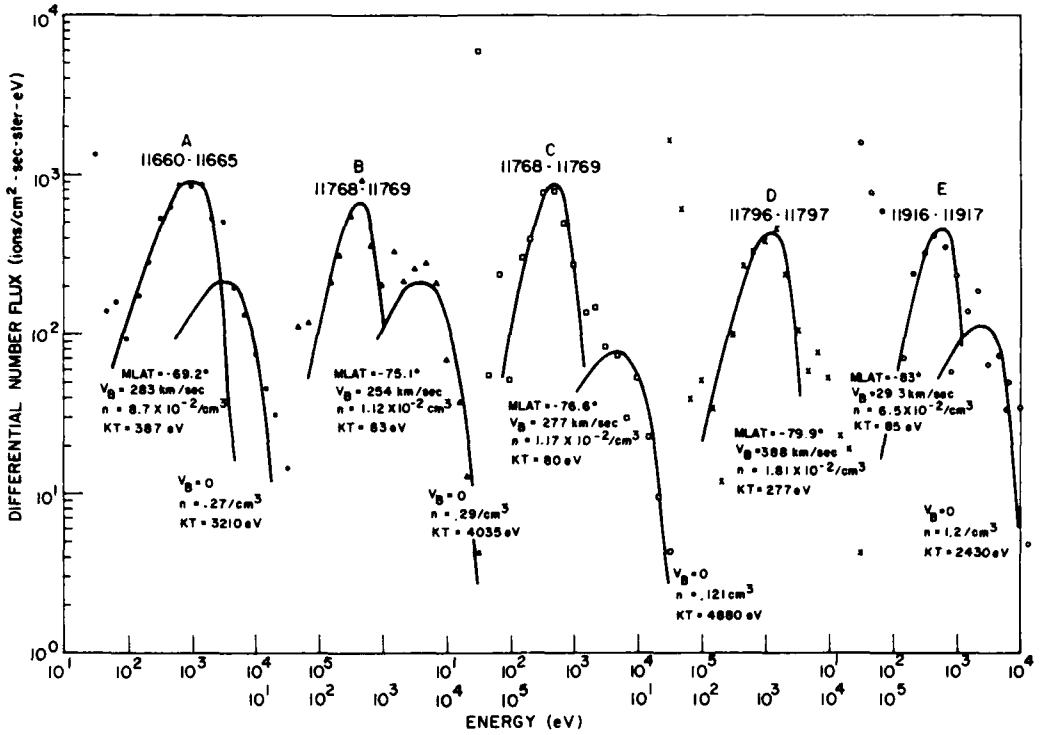

Fig. 15. Selected ion spectra observed in the current region I marked in Plate 3.

The one exception to this general behavior is seen in current region IV (Figure 18) where the ion spectrum at low energies is fit to a thermal maxwellian (kT_i = 500 to 1000 eV; n = 0.5 to 1.5 ions/cm^3). At higher energies the spectrum had either a high-energy tail consistent with a second hotter thermal population or a secondary peak consistent with a flowing ion population. The fit characteristics for the ions in current region IV alone are consistent with a possible plasma sheet source.

Despite the overall similarity of the ion spectral character-

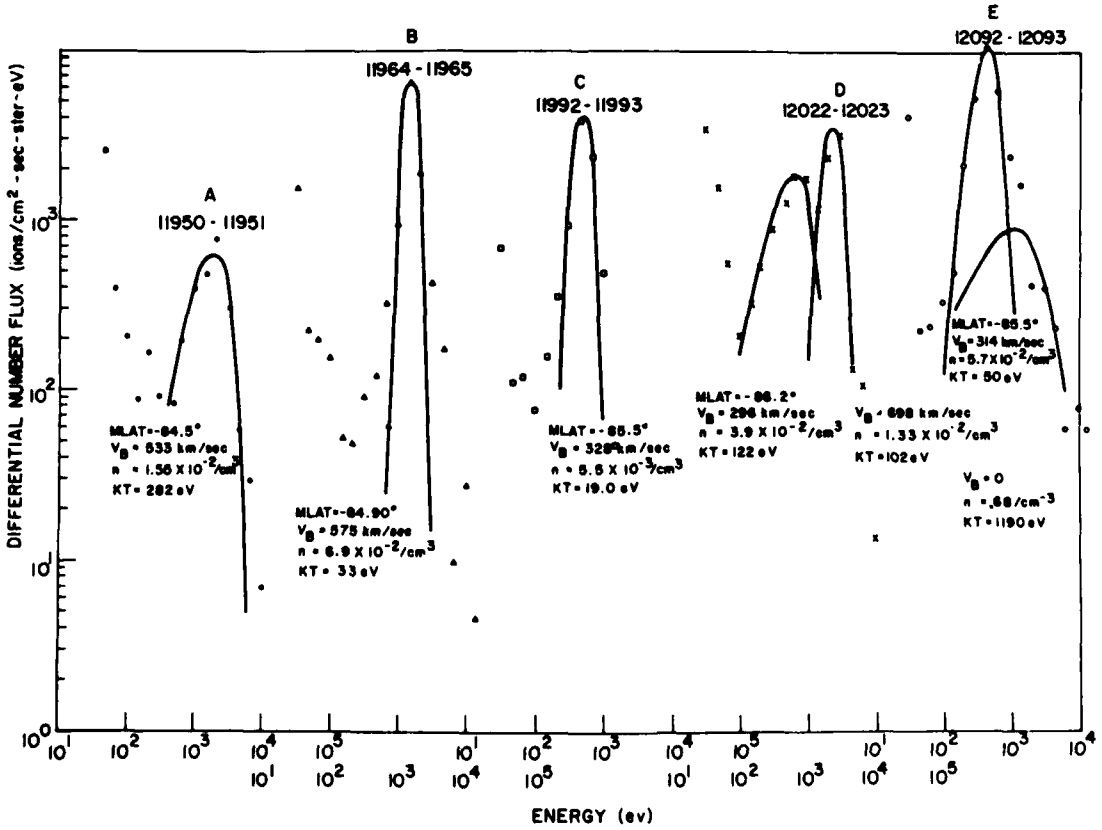

Fig. 16. Selected ion spectra observed in the current region II marked in Plate 3.

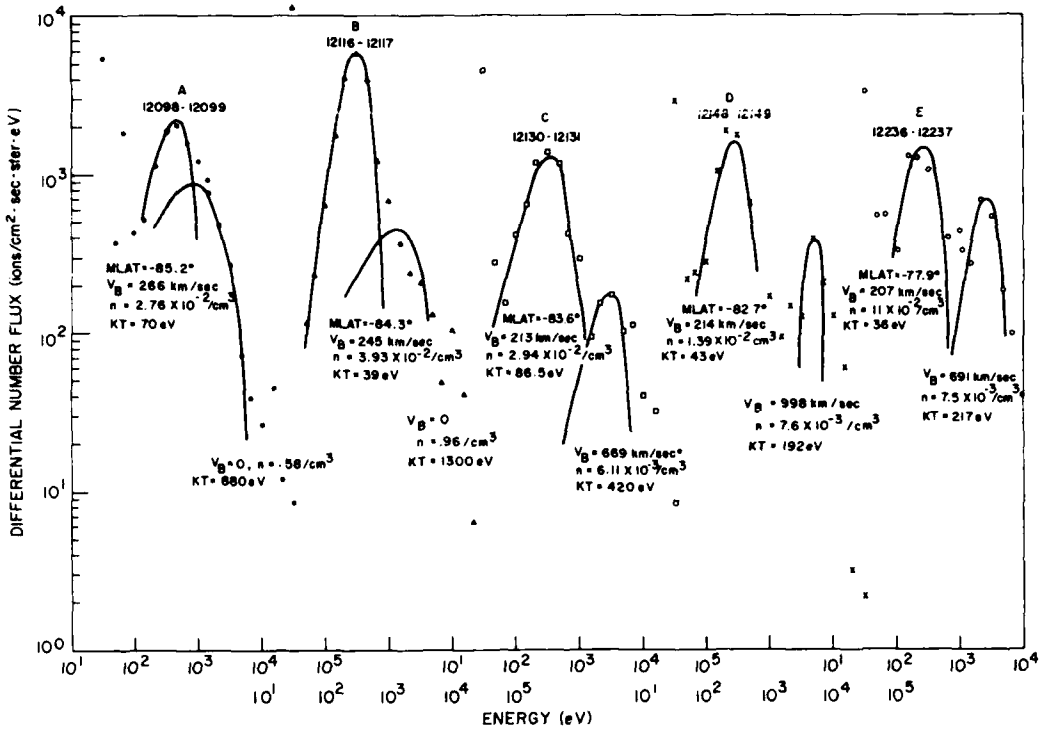

Fig. 17. Selected ion spectra observed in the current region III marked in Plate 3.

istics throughout the BPR there is one significant variation that deserves comment. Referring to the color spectrogram (Plate 3), one notes that throughout current region II (Figure 16) and part of current region III (Figure 17), the flux level at the ion peak increased. In addition, in this interval the energy of the peak varied with latitude and/or time in a consistent manner. This shift in the energy of the ion peak is found to reflect a dispersion in latitude and/or time of the inferred bulk velocity of the ions.

This dispersion can be seen in the fitted spectra. Starting at approximately the equatorward boundary of current region II the inferred bulk velocity increased, reaching a maximum of approximately 575 km/s. For some of the spectra both the peak intensity and the width of the spectrum cannot both be fit simultaneously by a simple flowing maxwellian. For these cases we fit to the peak, which tends to underestimate both the temperature and the number density. From 11964 to 11996 s UT, the ion peak shifted to lower energies reflecting a dispersion with increasing latitude in the inferred bulk velocity from values of 575 km/s to 300 km/s. The smallest bulk velocity was observed approximately coincident with the reversal in the sign of the ΔB_z component. Between 11996 and 12010 s UT the location of the peak in the ion spectrum fluctuated in the energy range from 300 eV to 1 keV before stabilizing at 600 eV. Starting at 12014 s UT a second peak begins to be noticeable at energies of approximately 3 keV with the intensity of the second peak quickly exceeding that of the lower-energy peak (spectrum D, Figure 16).

Such double peaked spectra occurred continuously from 12014 to 12064 s UT in current region II. In this interval the low-energy peak shifted to ~1 keV while the high-energy peak shifted downward in energy to ~2 keV. The shift in the high energy peak again reflects a dispersion in the inferred bulk velocity. No consistent ratio in the inferred bulk velocities for the two ion populations was maintained. After 12064 s UT only a single peaked spectrum was observed with either the suggestion of a weak peak at higher energies or a high-energy tail that can be approximated by a thermal Maxwellian distribution. In this interval the peak continued to shift to lower energies, reflecting a continuing decrease in the inferred bulk velocity.

Referring to Figure 12 one notes that for the NBZ pass the satellite was traveling at an angle of approximately 45° to the noon-midnight meridian. As such there would be a sunward component to the ΔB vector whenever the ΔB_z component was positive or whenever the ΔB_z component was negative and the ΔB_y component was positive and greater in magnitude than the ΔB_z component. Referring to Plate 3 one can see that the ΔB vector first had a sunward component approximately coincident with the boundary of current region II and that it retained a sunward component well into current region III. This region of a sunward component of the ΔB vector was coincident with the region in which were observed the increase in peak intensity and the velocity dispersions. For the south pole the ΔB vector is in the same direction as the convective plasma drift such that the dispersions were confined to the region of sunward convection.

Such velocity dispersions can have several sources. First they can result from an impulsive injection at a distant point along the field line, in which case the dispersion reflects the difference in transit time for ions of different energies from the injection point to the point of observation. Second, they can arise due to a velocity filter effect of the convection electric field. For a spatially confined source region, ions with lower energies will be observed at greater cross-field distances from the source region since they will have longer transit times along the magnetic field from the source region, which in turn allows them to be convected a longer distance across the field lines. Lastly, the dispersion could result from a combination of the two. Which of these processes leads to the dispersion observed cannot be determined using data from a single satellite. Despite this we can say, at least, that the process populating the sunward convecting field lines with magnetosheath-type ions differs significantly from the process operating on the antisunward convecting field lines. This point will be considered in the discussion section.

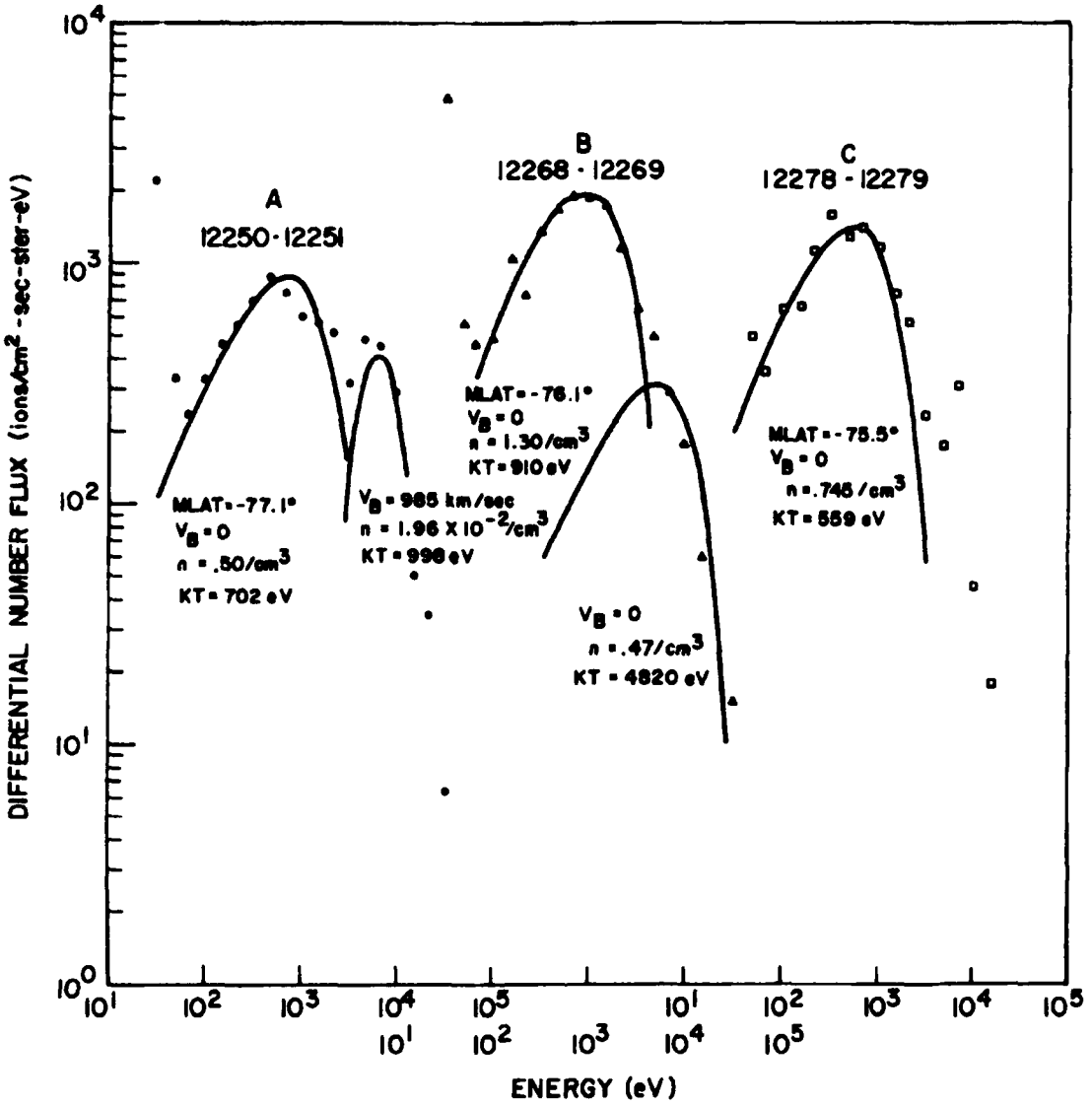

Fig. 18. Selected ion spectra observed in the current region IV marked in Plate 3.

3.3. *Summary of Observations*

During a period when the solar wind plasma was hotter, denser and faster flowing than normal, the interplanetary magnetic field turned strongly northward near 0000 UT on February 8, 1986 and remained strongly northward until 0406 UT. The observations from the DMSP and HILAT satellites in low polar orbit indicate a reconfiguration of the magnetosphere similar to, but stronger than, other reported periods of northward IMF.

While the IMF B_z was strongly positive, the equatorward boundary of CPS electron precipitation and the poleward boundary of BPR electron precipitation both moved strongly poleward. The boundary between the CPS and BPR electrons did not move significantly. This resulted in the shrinking of the region of CPS electrons and the growth of the region of BPR electrons. The shrinking of the electron CPS region was coincident with the disappearance of the auroral zone region 1/2 currents, and the expansion of the BPR occurred simultaneously with the appearance of the NBZ current system in the southern (summer) polar region. The NBZ currents appear to have expanded from the dayside toward the nightside and were entirely embedded in the BPR. The NBZ currents were not current sheets in the sense of the "infinite current sheet approximation," but were current regions. In the northern (winter) polar region, an irregular distribution of large field-aligned currents was observed that is inconsistent with the expected NBZ patterns. Their location did not correlate with the CPS/BPR or BPR/PC boundaries.

The precipitating electrons within the BPR in the southern hemisphere, where the NBZ currents were observed, had a single source population of relatively cool, high-density electrons. Variations in electron spectra were primarily due to field-aligned potentials related to small-scale current sheets and polar cap arcs. A detailed inspection of the data shows that in three of the four current regions, the source populations of the ions had BPR characteristics. There were typically two components: a low-energy component of flowing ions and a higher-energy, more thermal population that carried most of the ion number and energy density flux. The ion population with the fastest flow was found in current region II, which was a downward current region. Velocity dispersions were observed across the region of sunward convection. The ions in current region IV, the one closest to the dayside and morningside, had characteristics consistent with a CPS origin. The apparently different origin of the ions and electrons in region IV is a fact that must be explained by considering the different mobilities and by con-

sidering the dynamics and structure of the magnetospheric boundary region.

4. DISCUSSION

In the preceding sections, we have analyzed in detail the characteristics of the precipitating particles and magnetic field at high latitudes and low altitudes for a period of IMF B_z strongly positive during the geomagnetic storm of February 7-10, 1986. In this section we will discuss the following aspects of this characterization: (1) With the sharp northward turning of the IMF, there was a marked poleward expansion of the boundary plasma region (BPR) such that the poleward boundary of the BPR eventually reached close to the geomagnetic pole. (2) In both hemispheres the region 1 / region 2 current system died out, and in the sunlit south pole an NBZ current system was observed, embedded in the expanded BPR. (3) At latitudes above the CPS/BPR boundary, bright Sun-aligned arcs occurred in both the BPR and in regions where the electron and ion fluxes were at a baseline level normally associated with the polar rain. The characteristics of the electrons and ions in the arcs in the two regions were the same. Nowhere in the region above the CPS/BPR boundary were there hot electrons or ions with characteristics of the central plasma sheet. (4) While the data indicate sunward convection at very high latitudes in association with the NBZ system, there is no evidence for a multicell convection pattern or bifurcation of the geomagnetic tail. (5) The difference in the field-aligned current and convection pattern between the two hemispheres seems to be more fundamental than a difference in summer/winter conductivity levels.

To our knowledge this is the first report where the characteristics of the particle precipitation have been determined throughout the NBZ current system. In previous work, where only the magnetic field was measured, the authors have either implied or explicitly stated that much of the NBZ current system lies at latitudes poleward of the latitudinally continuous region of auroral precipitation [*Iijima et al.*, 1984; *Iijima and Shibaji*, 1987; *Bythrow et al.*, 1985], i.e., above the CPS and BPR. We have shown, however, at least for this one case that the NBZ occurrence corresponds instead with an increase in the width and poleward extent of the BPR.

The collocation of much of the NBZ current system with the expanded BPR has important implications as to the processes generating these currents. In particular, it ties the current generation to processes taking place in the boundary regions of the magnetosphere. Since the prominent NBZ pattern is seen to the dayside of the high-latitude ionosphere/magnetosphere, this implies that the NBZ system maps to the low-latitude boundary layer and/or the cusp/cleft. This association is clearly supported by the fact that the electron and ion populations in the BPR uniformly have magnetosheathlike characteristics. We attribute the observed variation in ion spectral characteristics to velocity filter effects operating on the ion distribution between its source in the boundary region and its detection at low altitudes.

In regions with weak gradients in the ionospheric conductivity, such as the summer polar ionosphere, ΔB is proportional to and parallel (for southern hemisphere) or antiparallel (for northern hemisphere) to the ion drift velocity or $E \times B$. Thus we are able to state that a portion of the NBZ current system lies in a region of sunward convection (see Figure 12). *Bythrow et al.* [1985] have associated this region of sunward convection inferred from the ΔB with the region of sunward convection reported in the theta aurora [*Frank et al.*, 1986]. Based upon particle characteristics and in particular the presence of precipitating O^+ some researchers have hypothesized that the central plasma sheet is the source for the particles in the theta aurora [*Frank et al.*, 1982; 1986; *Peterson and Shelley*, 1984]. This has led to theories in which the tail lobe is bifurcated by a channel of closed field lines populated by central plasma sheet particles. For the event studied here, the particle characteristics do not support the idea of the sunward convection zone being associated with the plasma sheet. Rather the uniformly cold electron spectrum and the implied flow in the ions is more consistent with a thickening of the dayside boundary regions in the magnetosphere. In particular, we note no major variation in the precipitating electron particle characteristics in regions of sunward and antisunward convection, and nowhere in the high-latitude portion did we observe an electron or ion spectrum that would indicate a central plasma sheet origin. We also note that within both the sunward and antisunward convection zones populated by BPR particles there were numerous acceleration regions that we associate with Sun-aligned, trans-polar-cap arcs. These arcs all occurred on spatial scales much smaller than the regions of sunward and anti-sunward convections and there is no variation in the characteristics of these acceleration regions in the sunward and anti-sunward convection zones. This association of the arcs with magnetosheath-type particles is consistent with the work of *Burke et al.* [1982] and *Hardy et al.* [1982]. Such an expansion of the BPR is also consistent with work of *Makita and Meng* [1984] where they showed that generally a significant thickening of the BPR occurs in response to a northward IMF B_z component.

Observations of sunward convection at very high latitude have led to models of three and four convection cells in the ionospheric/magnetospheric system [e.g., *Reiff and Burch*, 1985; *Heelis et al.*, 1986]. These researchers propose that the central cell(s) map to open field lines in the magnetotail lobes which merge on the dayside with the IMF. This merging produces sunward convection in the central polar cap and lobe region. In such a model there is little or no merging of closed field lines with the IMF. The equatorward cells in the multicell model map to closed field lines driven by "viscous" interactions in the boundary layer. For this case the level of precipitating flux in the sunward convecting region at very high latitudes would be at a minimum since most of the magnetosheath plasma injected onto the open geomagnetic field line during the merging would be convected into the field lines of the distant magnetotail. The result would be that the sunward-convecting, open flux tubes would contain few particles. For the case we presented here this is clearly not the case. The antisunward convection region of the "viscous" cell maps to the low-latitude boundary layer. The particle data for this region clearly show BPR plasma, but, since the potential across the "viscous" region cannot exceed a few kilovolts, it seems improbable for the "viscous" region to be the source of the wide convection region observed in the evening leg of the "W" pattern observed in the 0308 UT pass of F7. (The electric field in the boundary layer is estimated from measured parameters; if the boundary layer thickness is a few ion gyroradii or less, then the "viscous" potential is 5 kV or less.)

Since the characteristics of this event do not support either a "bifurcated tail" pattern for convection or a multicell convection pattern, we are left with the question of what is the convection pattern. While multicell convection patterns are widely suggested for northward IMF periods, they are not universally supported. For example, *Friis-Christensen et al.* [1985], *Heppner and Maynard* [1987] and *Crooker* [1988] have provided data and theory to support a distorted two-cell convection pattern during periods of northward IMF. In particular, *Crooker* [1988, 1989] has stated

that the ionospheric/magnetospheric convection is driven by merging of closed geomagnetic field lines for all orientations of the IMF.

We examined *Crooker's* [1988] model to see how well it can account for our observations. In Plate 4 we show a slightly modified version of the Crooker model for IMF $B_z > 0$ and IMF $B_y > 0$. (Plate 4 is shown here in black and white. The color version can be found in the separate color section in this issue.) In the figure we include the orbital track of the F7 satellite pass displaying the maximum NBZ current marked with the location of the four current regions. In addition, we show the extent of the various plasma regions, the boundary between open and closed field lines and the cusp location. Note that this convection pattern is similar to that proposed by *Heppner and Maynard* [1987] for northward IMF although the Heppner-Maynard model predicts return currents which are not in our data. More importantly one can see that such a pattern does reproduce the 4 components of the W pattern associated with the NBZ current system.

The configuration in Plate 4 also suggests an explanation as to why the CPS/BPR boundary does not move significantly during this period. As the IMF turns from southward to northward, the merging zone and the boundary between open and closed field lines rotate rather than immediately shrinking toward the pole. If the "open/closed" boundary does not move significantly, the CPS/BPR boundary also will not move significantly. The equatorward edge of the plasma sheet shrinks poleward as the electric field in the inner magnetosphere decreases in strength, and the inner edge of the central plasma sheet moves outward. These findings are consistent with those of *Gussenhoven and Mullen* [1989] where they used MeV electrons ejected from the sun and entering the high-latitude region through the open field line of the magnetotail to trace the region of open/closed field lines. They also found that the boundary between open and closed field lines change little when the IMF became northward while the poleward boundary of the BPR moved poleward.

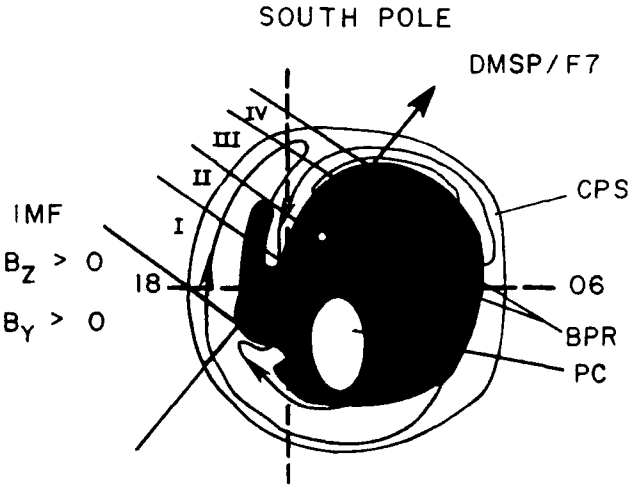

Plate 4. Estimated configuration of the ionospheric convection pattern and its relationship to the precipitating particle regions observed in the southern high-latitude region during the NBZ passes of DMSP F7. The southern polar region is shown as seen through a "glass" earth to aid in the comparison with northern polar region diagrams. The diagonal line from lower left to upper right represents the path of DMSP F7 through the pattern. The diagonal lines intercepting the DMSP F7 path mark the boundaries between regions as shown in Plate 3. The heavy, solid line represents the boundary between open and closed field lines. The open circle is the ionospheric projection of the cusp. The closed circles map to the edges of the merging region on the magnetopause. The regions of CPS and BPR precipitating electrons are shaded and marked. The unshaded region within the open field line region maps to the lobes of the geomagnetic tail. The color version of this figure can be found in the separate color section in this issue.

Such a model also explains the velocity dispersions observed in current regions II and III. In Plate 4 one notes that current regions II and III are poleward of the merging region. For ions injected and/or accelerated at the merging region, dispersions in the sense measured would be observed with increasing distance from the merging region since in this case the satellite is traveling approximately parallel to the convection velocity vector. The multiple peaks in the ion spectrum we interpret as arising from a variation in the location of the merging region and/or from sporadic merging.

Such a model does not explain the large latitudinal extent of the BPR. In Plate 4 we show the BPR extending over a wide area of open as well as closed field lines. BPR plasma should be seen primarily on field lines that map to the dayside of the magnetosphere where there is a significant component of the ion flow velocity along the magnetic field into the ionosphere. For field lines mapping into the tail, the ion flow at the magnetopause is antisunward, and few electrons or ions will have sufficient energies to counterstream into the ionosphere against the prevailing flow. We believe it unlikely that field lines up to the geomagnetic pole all map to the dayside magnetopause.

Alternately we speculate that the large latitudinal extent of the BPR could be explained if there was a kink (a region of small radius of curvature) in the open field line at the magnetopause produced from the merging process. Such a kink could operate to trap plasma on open field lines as the plasma is convected from field lines connecting to the dayside magnetopause to those field lines mapping to the flanks of the magnetotail. The process producing such a kink on the field line might be similar to the "flux transfer events" seen for periods of southward IMF [see *Cowley* [1982] and references therein]. The convection patterns for northward and southward IMF are different, but the merging process on closed field lines should be similar.

The unshaded area in Plate 4 represents the region of nearly empty flux tubes within the magnetosphere and is identified in the precipitating electron data as the "polar cap." We propose that these flux tubes are empty because the kink has straightened out enough to release the plasma, the plasma on the trapped portion of the field line has been exhausted, or these flux tubes follow a convection pattern that never brings them to either the merging or reconnection region. We have placed the PC region so that all passes of DMSP F6 (Figures 6 and 7) and the northern hemisphere passes of DMSP F7 (Figure 8) will observe this region while the southern hemisphere pass of DMSP F7 at $\sim$ 0320 UT will miss this region. In other words, we suggest that the failure to observe the PC region at very high latitudes (Figure 9) does not imply that the PC region does not exist but only that it is small and asymmetric with respect to the magnetic pole.

If a significant portion of the flux tubes maintain the kink at the magnetopause until they reach the reconnection region in the magnetotail, then a large portion of the magnetotail will be filled with boundary-type plasma as we observed. This still leaves the question of the source of plasma for the "polar cap arc" observed by DMSP F6 in the PC region. The arcs which we have shown result from both an increase in field-aligned energy due to a field-aligned potential and a density enhancement in the source region. We speculate

that these flux tubes were filled with BPR plasma as they merged with the IMF, and due to some process, the plasma in them was not lost as quickly as plasma in adjacent flux tubes. Possibly these flux tubes have convected away from the merging region faster than adjacent flux tubes and have had less time for the plasma to be lost. This requires uneven convection and/or uneven merging on the magnetopause; two conditions which are possible. The plasma may also be held in these open flux tubes by an electrostatic barrier related to the electrostatic potential accelerating the electrons.

We also noted that the observed field-aligned currents in the northern hemisphere differed from the NBZ current system in the southern hemisphere. *Bythrow et al.* [1985] have suggested that the difference is entirely due to a difference in conductivities. They have argued that low ionospheric conductivity in the dark hemisphere cause an irregular pattern of currents for scale sizes less than 600 km (40 s of DMSP flight time), while the NBZ system is maintained at longer scale lengths. If this suggestion held, we would find a region of sunward convection (and antisunward ΔB) near the center of the cap with antisunward convection (and sunward ΔB) on the dusk and dawn sides of the cap. We do not see the signature of NBZ current and convection pattern in the northern hemisphere pass (Figure 8) at these longer scale lengths even if we compensate for the difference in conductivity. Overall, the sheet current strengths (amperes per meter) are smaller in the northern hemisphere than the summer hemisphere by a ratio similar to the solar UV induced conductivity ratio. This implies that the large-scale electric field has approximately the same magnitude in both hemispheres. We also note that the most irregular field-aligned currents are found in the twilight zone between 0223 and 0225 UT. Thus the small-scale irregularities may be related to the ionospheric conductivity gradient.

The configuration shown in Plate 4 provides a partial explanation for the difference in current patterns between the poles. In Plate 4, the convection pattern and the associated field-aligned currents are very asymmetric with respect to both the noon-midnight and dusk-dawn meridians. If the pattern in Plate 4 is transposed about the noon-midnight meridian to give the expected pattern in the north pole, then the merging region would map to the afternoon quadrant. For this case DMSP F7 does not pass through current and convection regions that would give the "W" pattern in the magnetometer data. Rather the pass is well away from regions of rapid convection and large currents. This would explain why the field-aligned currents are small in the first part of the pass (before 0223 UT) when the ionosphere was illuminated. On the other hand this suggestion requires that a NBZ configuration be present (with diminished strength due to the conductivity difference) in the dayside portion of the winter polar region. The lack of any such report may be used to argue against such a configuration, but it is not clear that sufficient studies have been done to rule out our suggestion.

5. CONCLUSIONS

1. The existence of northward IMF causes a decrease in the area of CPS precipitation over a period of hours, if the northward direction is maintained. This occurs as the auroral oval decreases in radius. At the same time the area of BPR precipitation increases, almost exclusively by means of poleward expansion. This implies a decrease in the volume of the plasma sheet and an increase in the volume of the boundary plasma regions in the magnetosphere. The expanded BPR region and the NBZ current system collocate in the south pole.

2. The location of boundaries between precipitation regions is independent of hemisphere throughout the period of northward IMF. This implies that both the north (winter) and south (summer) high-latitude ionospheres are connected to the same regions in the magnetosphere. However, there are distinct differences in the field-aligned currents observed in the two polar ionospheres which cannot be explained by the difference in ionospheric conductivity. If the two polar regions are connected to the same regions in the magnetosphere, the manner of the connection must be different.

3. The boundary between CPS electron precipitation and BPR electron precipitation is not as significantly affected by the northward turning of the IMF as the equatorward boundary. This may indicate that the boundary between open and closed field lines changes slowly such that much of the BPR electron precipitation observed while the IMF was northward was observed in regions of open field lines.

4. The source region for the NBZ currents observed on February 8, 1986 was in the boundary plasma region, not the polar cap or plasma sheet. This indicates that a bifurcation of the tail did not occur.

5. Polar cap arcs are observed both in the BPR and the PC precipitating electron regions. The polar cap arcs are not directly related to the NBZ currents nor to boundaries between BPR and polar cap region. There is no evidence that the source of the polar cap arc is an intrusion of CPS plasma into very high latitudes.

6. Plasma flow vectors inferred from the magnetic field data better fit a distorted two cell convection pattern than a multicell pattern. We propose that the power for the ionosphere/magnetosphere activity during northward IMF comes from merging with closed field lines, and not from merging of open field lines.

7. There is a growth time for the expansion of the region of the NBZ currents and the increase in strength. The decay time for the NBZ currents after the IMF turns southward is much shorter than the growth time.

Acknowledgments. Analysis of DMSP data is supported by the Air Force Office of Scientific Research under task 2311G5. The DMSP magnetometer was built and calibrated by the Applied Physics Laboratory of Johns Hopkins University under the direction of Dr. T. A. Potemra. Interplanetary magnetic field data from IMP 8 were provided by R. Lepping.

The Editor thanks T. S. Jorgensen and P. E. Sandholt for their assistance in evaluating this paper.

REFERENCES

Allen, J. H., Major magnetic storm effects noted, *Eos, Trans. AGU, 67*, (25), 537, 1986.

Burke, W. J., M. C. Kelley, R. C. Sagalyn, M. Smiddy, and S. T. Lai, Polar cap electric field structures with a northward interplanetary magnetic field, *Geophys. Res. Lett., 6*, (1), 21–24, 1979.

Burke, W. J., M. S. Gussenhoven, M. C. Kelley, D. A. Hardy, and F. J. Rich, Electric and magnetic fields characteristics of discrete arcs in the polar cap, *J. Geophys. Res., 87*, (A4), 2431–2443, 1982.

Bythrow, P. F., W. J. Burke, and T. A. Potemra, Ionospheric evidence for irregular reconnection and turbulent plasma flow in the magnetotail during periods of northward interplanetary magnetic field, *J. Geophys. Res., 90*, (A6), 5319–5325, 1985.

Cowley, S. W. H., The causes of convection in the Earth's magnetosphere: a review of developments during the IMS, *Rev. Geophys., 20*, (3), 531–565, 1982.

Crooker, N. U., Mapping the merging potential from the magnetopause to the ionosphere through the dayside cusp, *J. Geophys. Res., 93*, (A7), 7338–73344, 1988.

Crooker, N. U., Magnetospheric topology on IMF orientation, in *Physics of Space Plasmas (1987): Proceedings of 1987 Workshop, Ionosphere-Magnetosphere-Solar Wind Coupling Processes*, edited by T. Chang, G. R. Crew, and J. R. Jasperse, pp. 127–136, Scientific Publishers, Cambridge, Mass., 1989.

Eastman, T. E., L. A. Frank, and C. Y. Huang, The boundary layers as the principal transport region of the Earth's magnetotail, *J. Geophys. Res.*, *90*, (A10), 9541-9560, 1985.

Eather, R. H., DMSP calibration, *J. Geophys. Res.*, *84*, (A8), 4134-4144, 1979.

Frank, L. A., J. D. Craven, J. L. Burch and J. D. Winningham, Polar views of the earth's aurora with Dynamics Explorer, *Geophys. Res. Lett.*, *9*, (9), 1001-1004, 1982.

Frank, L. A., J. D. Craven, D. A. Gurnett, S. D. Shawhan, D. R. Weimer, J. L. Burch, J. D. Winningham, C. R. Chappell, J. H. Waite, R. A. Heelis, N. C. Maynard, M. Sugiura, W. K. Peterson, and E. G. Shelley, The theta aurora, *J. Geophys. Res.*, *91*, (A3), 3177 3224, 1986.

Friis-Christensen, E., Y. Kamide, A. D. Richmond, and S. Matsushita, Interplanetary magnetic field control of high-latitude electric fields and currents determined from Greenland magnetometer data, *J. Geophys. Res.*, *90*, (A2) 1325-1338, 1985.

Gussenhoven, M. S., Extremely high latitude auroras, *J. Geophys. Res.*, *87*, (A4), 2401-2412, 1982.

Gussenhoven, M. S., Low-altitude convection, precipitation and current patterns in the baseline magnetosphere, *Rev. Geophys.*, *26*, (4), 792-808, 1988.

Gussenhoven, M. S., and E. G. Mullen, Simultaneous relativistic electron and auroral particle access to the polar caps during IMF B_z northward: A scenario for an open field line source of auroral particles, *J. Geophys. Res.*, *94*, (A12), 17,121-17,132, 1989.

Gussenhoven, M. S., D. A. Hardy, and N. Heinemann, Systematics of the equatorward diffuse auroral boundary, *J. Geophys. Res.*, *88*, (A7), 5692-5708, 1983.

Gussenhoven, M. S., D. A. Hardy, N. Heinemann, and R. K. Burkhardt, Morphology of the polar rain, *J. Geophys. Res.*, *89*, (A11), 9785-9800, 1984.

Gussenhoven, M. S., D. A. Hardy, and N. Heinemann, The equatorward boundary of the auroral ion precipitation, *J. Geophys. Res.*, *92*, (A4), 3273-3283, 1987.

Hardy, D. A., Intense fluxes of low energy electrons at geomagnetic latitudes above 85 degrees, *J. Geophys. Res.*, *89*, (A6), 3883-3892, 1984.

Hardy, D. A., W. J. Burke, and M. S. Gussenhoven, DMSP optical and electron measurements in the vicinity of polar cap arcs, *J. Geophys. Res.*, *87*, (A4), 2413-2430, 1982.

Hardy D. A., L. K. Schmitt, M. S. Gussenhoven, F. J. Marshall, H. C. Yeh, T. L. Schumaker, A. Huber, and J. Pantazis, Precipitating electron and ion detectors (SSJ/4) for the block 5D/flight 6-10 DMSP satellites: calibration and data presentation, AFGL-TR-84-0314, Air Force Geophys. Lab., Hanscom Air Force Base, MA, 1984a.

Hardy, D. A., A. Huber, and J. A. Pantazis, The electron flux J sensor for HILAT, *APL Tech. Dig.*, *5*, 125-130, 1984b.

Hardy, D. A., M. S. Gussenhoven and E. Holeman, A statistical model of auroral electron precipitation, *J. Geophys. Res.*, *90*, (A5), 4229-4248, 1985.

Heelis, R. A., P. H. Reiff, J. D. Winningham, and W. B. Hanson, Ionospheric convection signature observed by DE 2 during northward interplanetary magnetic field, *J. Geophys. Res.*, *91*, (A5), 5817-5839, 1986.

Heikkila, W. J., The morphology of auroral precipitation, *Space Res.*, *12*, (2), 1343-1355, 1972.

Heppner, J. P., and N. C. Maynard, Empirical high-latitude electric field models, *J. Geophys. Res.*, *92*, (A5), 4467-4489, 1987.

Hoffman, R. A., M. Sugiura, N. C. Maynard, R. M. Candey, J. D. Craven, and L. A. Frank, Electrodynamic patterns in the polar region during periods of extreme magnetic quiescence, *J. Geophys. Res.*, *93*, (A12), 14515-14541, 1988.

Holzer, R. E., R. L. McPherron, and D. A. Hardy, A quantitative empirical model of the magnetospheric flux transfer process, *J. Geophys. Res.*, *91*,(A3), 3287-3293, 1986.

Iijima, T., and T. A. Potemra, The amplitude distribution of field-aligned currents at northern high latitudes observed by Triad, *J. Geophys. Res.*, *81*, 2165-2174, 1976.

Iijima, T., and T. Shibaji, Global characteristics of northward IMF associated (NBZ) field aligned currents, *J. Geophys. Res.*, *92*, (A3), 2408-2424, 1987.

Iijima, T., T. A. Potemra, L. J. Zanetti and P. F. Bythrow, Large-scale Birkeland currents in the dayside polar region during strongly northward IMF: A new Birkeland current system, *J. Geophys. Res.*, *89*, (A9), 7441-7452, 1984.

Ismail, S., D. D. Wallis, and L. L. Cogger, Characteristics of polar cap sun-aligned arcs, *J. Geophys. Res.*, *82*, (29), 4741-4749, 1977.

Lin, C. S., and R. A. Hoffman, Observations of inverted-V electron precipitation, *Space Sci. Rev.*, *33*, 415-457, 1982.

Makita, K., and C.-I. Meng, Average electron precipitation patterns and visual aurora characteristics during geomagnetic quiescence, *J. Geophys. Res.*, *89*, (A5), 2861-2872, 1984.

Meng, C. I., Simultaneous observations of low-energy electron precipitation and optical auroral arcs in the evening sector by the DMSP 32 satellite, *J. Geophys. Res.*, *81*, (16), 2771-2785, 1976.

Meng, C.-I., Polar cap arcs and the plasma sheet, *Geophys. Res. Lett.*, *8*, (3), 273-276, 1981.

Peterson, W. K., and E. G. Shelley, Origin of plasma in a cross-polar cap auroral feature (theta aurora), *J. Geophys. Res.*, *89*, (A8), 6729-6736, 1984.

Reiff, P. H., and J. L. Burch, IMF B_y dependent plasma flow and Birkeland currents in the dayside magnetosphere, 2. A global model for northward and southward IMF, *J. Geophys. Res.*, *90*, (A2), 1595-1609, 1985.

Rich, F. J., Fluxgate magnetometer (SSM) for the Defense Meteorological Satellite Program (DMSP) Block 5D-2, flight 7, Tech. Rep. AFGL-TR-84-0225, Air Force Geophys. Lab., Hanscom Air Force Base, Mass., 1984.

Rich, F. J., and M. S. Gussenhoven, The absence of region 1 / region 2 field-aligned currents during prolonged quiet times, *Geophys. Res. Lett*, *14*, (7), 689-692, 1987.

Riehl, K. B., and D. A. Hardy, Average characteristics of the polar rain and their relationship to the solar wind and the interplanetary magnetic field, *J. Geophys. Res.*, *91*, (A2), 1557-1571, 1986.

Vasyliunas, V. M., Interaction between the magnetospheric boundary layers and the ionosphere, Proceedings of Magnetospheric Boundary Layers Conference, Alpbach, 11-15 June 1979, *Eur. Space Agency Spec. Publ., ESA SP-148*, 387-393, 1979.

Whalen, B. A., J. R. Miller, and I. B. McDiarmid, Sounding rocket observations of particle precipitation in a polar-cap electron aurora, *J. Geophys. Res.*, *76* (28), 6847-6855, 1971.

Winningham, J. D. and W. J. Heikkila, Polar cap auroral electron fluxes observed with Isis 1, *J. Geophys. Res.* , *79*, (7), 949-957, 1974.

Winningham, J. D., F. Yasuhara, S.-I. Akasofu, and W. J. Heikkila, The latitudinal morphology of 10-eV to 10-keV electron fluxes during magnetically quiet and disturbed times in the 2100-0300 MLT sector, *J. Geophys. Res.*, *80*, (22), 3148-3171, 1975.

F. J. Rich, D. A. Hardy, R. H. Redus, and M. S. Gussenhoven, Space Physics Division, Geophysics Laboratory (AFSC), Hanscom Air Force Base, Bedford, MA 01731

(Received May 19, 1989;
revised September 12, 1989;
accepted September 15, 1989)

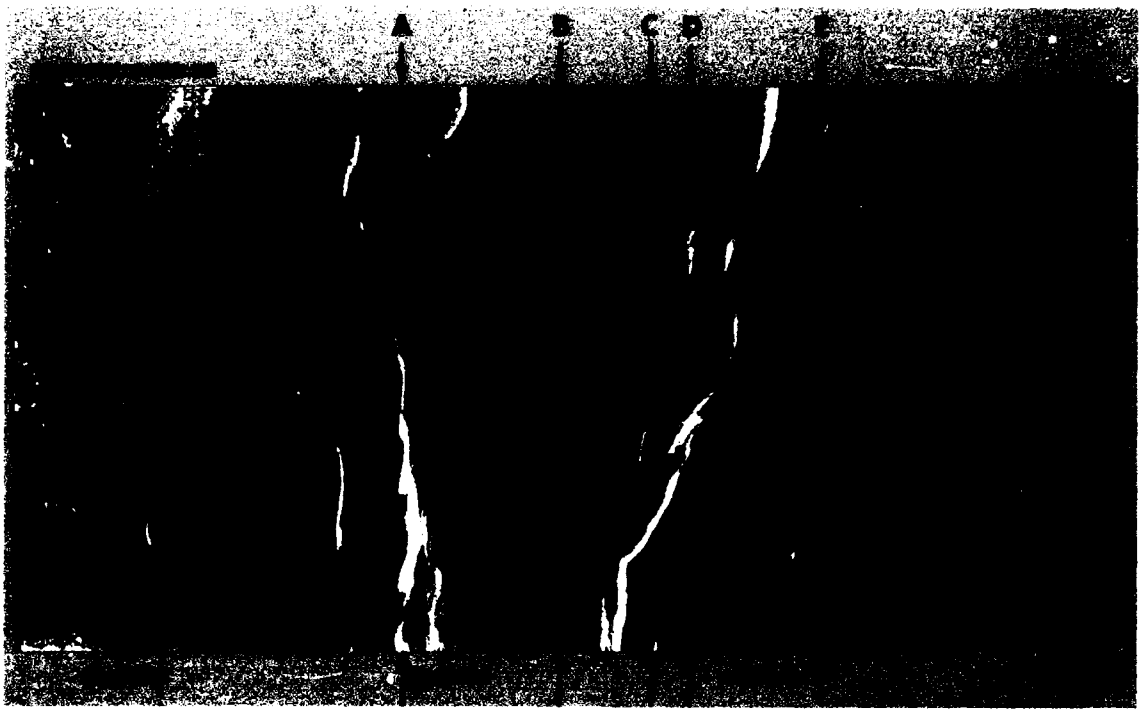

Plate 1 [*Rich et al.*]. False color reproduction of DMSP F6 white light imagery data obtained during the 0320–0341 UT pass through the northern (winter) high-latitude region. Numerous Sun-aligned, polar cap arcs are visible at very high latitudes. The satellite passed from left to right, and the imager scan lines are from the bottom to the top of the figure. The nadir look position has been marked with reverse color. Five visible arcs related to the electron flux enhancements marked in Figure 7 are labeled on the edge of the image with letters A through E.

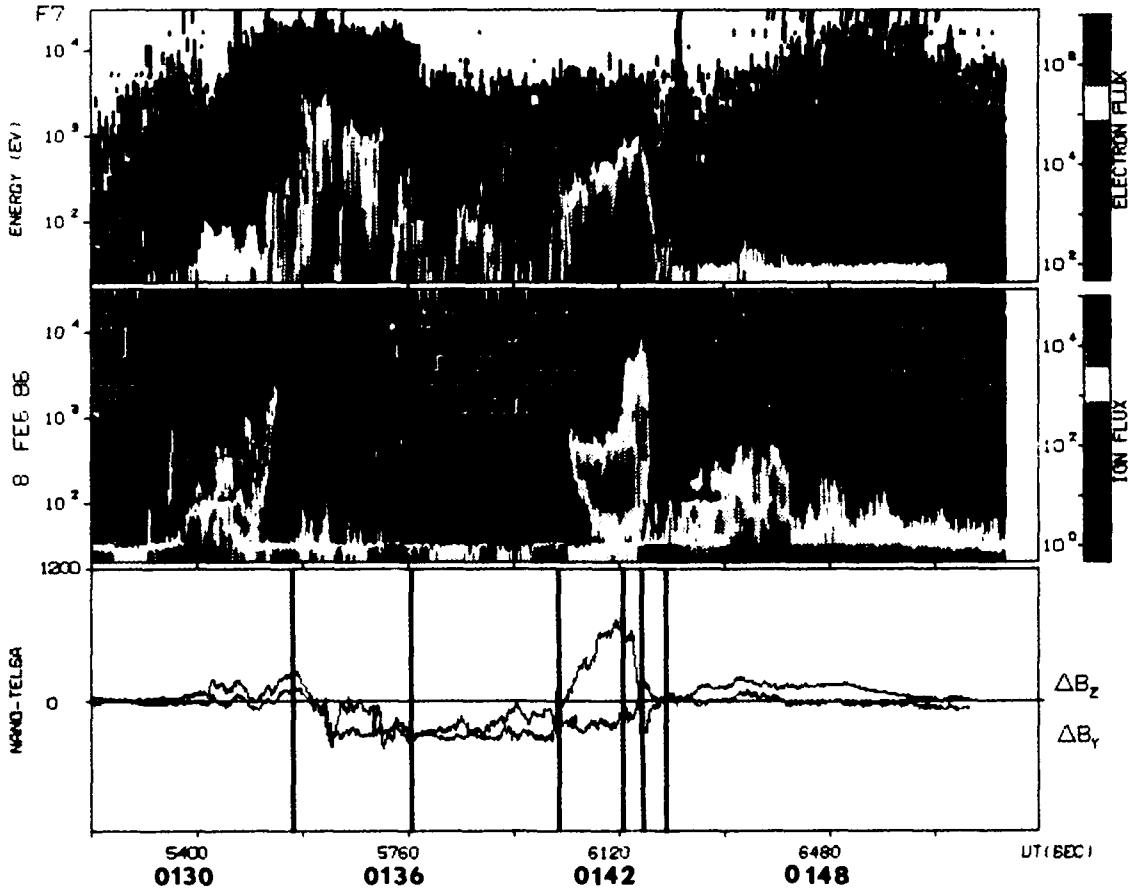

Plate 2 [*Rich et al.*]. DMSP F7 0127–0152 UT: Horizontal components of magnetic deflection (bottom panel) and spectrogram (top and middle panels) showing the distribution of electron and ion flux (color coded) versus energy (vertical axis) versus time (horizontal axis). The boundaries for the CPS, BPR and PC regions of particle precipitation are indicated with vertical lines. The partial NBZ current (0140–0143 UT) occurred entirely within the BPR.

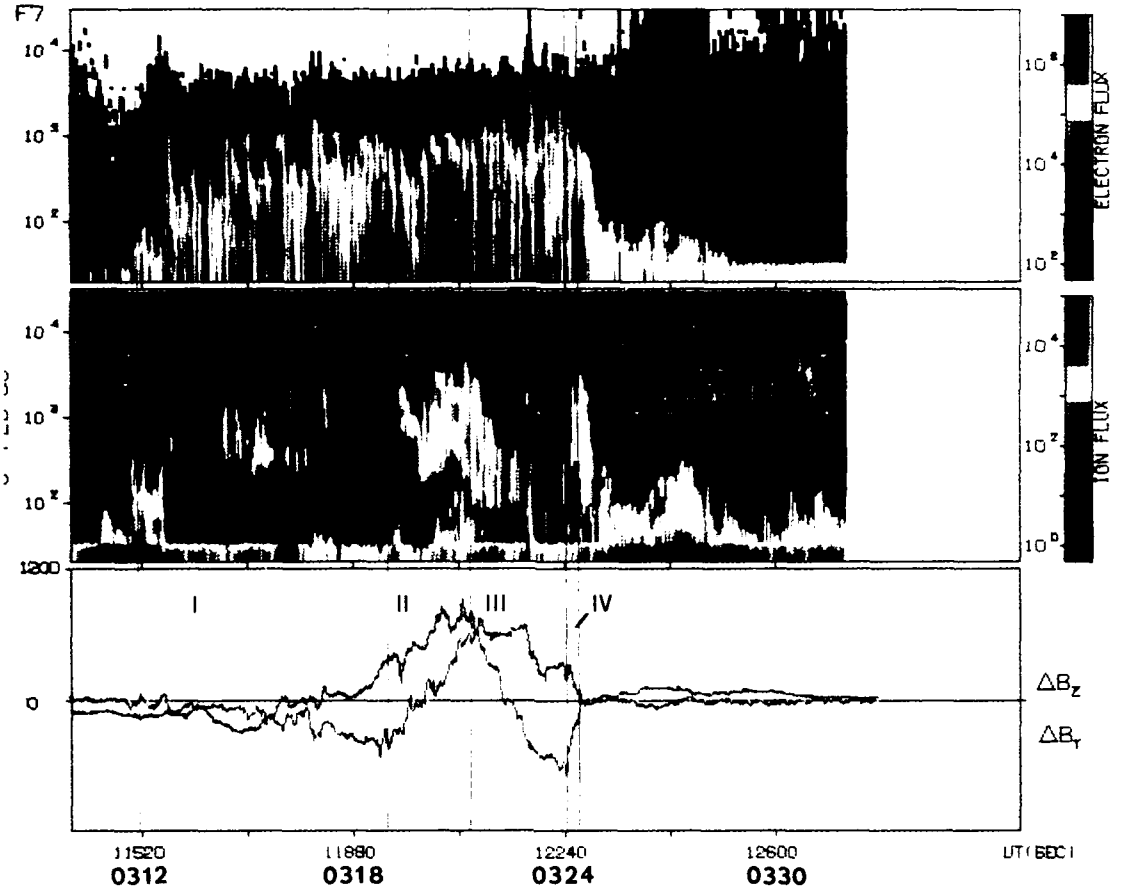

Plate 3 [*Rich et al.*]. DMSP F7 0308–0322 UT: Same format as Plate 2. The boundaries between the four NBZ current sheets or regions are indicated with vertical lines and the regions are denoted with roman numerals.

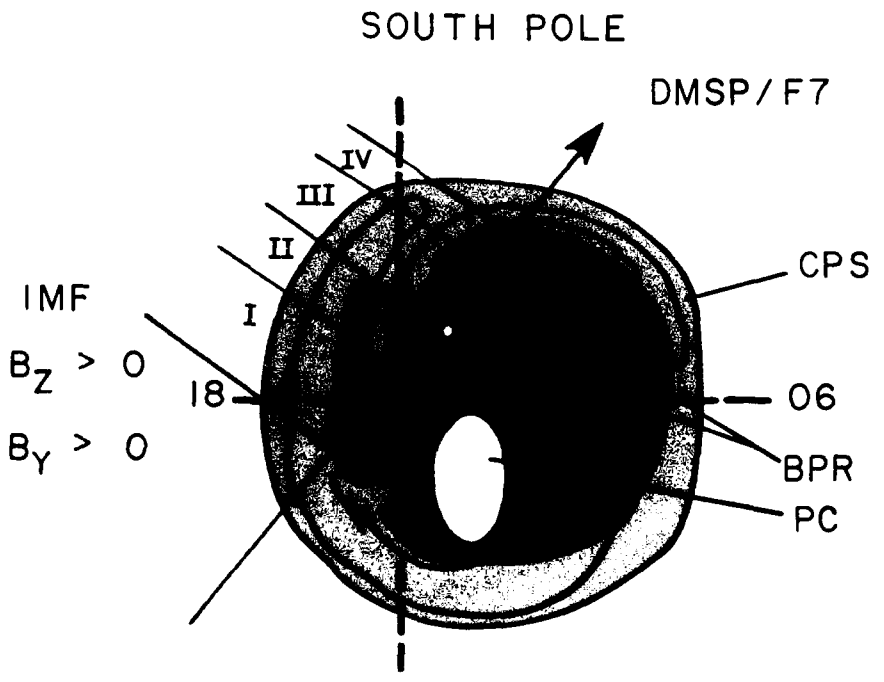

Plate 4 [*Rich et al.*]. Estimated configuration of the ionospheric convection pattern and its relationship to the precipitating particle regions observed in the southern high-latitude region during the NBZ passes of DMSP F7. The southern polar region is shown as seen through a "glass" earth to aid in the comparison with northern polar region diagrams. The diagonal line from lower left to upper right represents the path of DMSP F7 through the pattern. The diagonal lines intercepting the DMSP F7 path mark the boundaries between regions as shown in Plate 3. The heavy, solid line represents the boundary between open and closed field lines. The open circle is the ionospheric projection of the cusp. The closed circles map to the edges of the merging region on the magnetopause. The regions of CPS and BPR precipitating electrons are shaded and marked. The unshaded region within the open field line region maps to the lobes of the geomagnetic tail.